



National Library  
of Canada

Acquisitions and  
Bibliographic Services Branch

395 Wellington Street  
Ottawa, Ontario  
K1A 0N4

Bibliothèque nationale  
du Canada

Direction des acquisitions et  
des services bibliographiques

395, rue Wellington  
Ottawa (Ontario)  
K1A 0N4

*Your file - Votre référence*

*Our file - Notre référence*

## NOTICE

The quality of this microform is heavily dependent upon the quality of the original thesis submitted for microfilming. Every effort has been made to ensure the highest quality of reproduction possible.

If pages are missing, contact the university which granted the degree.

Some pages may have indistinct print especially if the original pages were typed with a poor typewriter ribbon or if the university sent us an inferior photocopy.

Reproduction in full or in part of this microform is governed by the Canadian Copyright Act, R.S.C. 1970, c. C-30, and subsequent amendments.

## AVIS

La qualité de cette microforme dépend grandement de la qualité de la thèse soumise au microfilmage. Nous avons tout fait pour assurer une qualité supérieure de reproduction.

S'il manque des pages, veuillez communiquer avec l'université qui a conféré le grade.

La qualité d'impression de certaines pages peut laisser à désirer, surtout si les pages originales ont été dactylographiées à l'aide d'un ruban usé ou si l'université nous a fait parvenir une photocopie de qualité inférieure.

La reproduction, même partielle, de cette microforme est soumise à la Loi canadienne sur le droit d'auteur, SRC 1970, c. C-30, et ses amendements subséquents.

UNIVERSITY OF ALBERTA

**Quantifying Scoliotic Shape Using Surface Curvature**

BY

Michael F. Polak



A thesis submitted to the Faculty of Graduate Studies and Research in partial fulfillment of the requirements for the degree of Master of Science.

DEPARTMENT OF ELECTRICAL ENGINEERING

Edmonton, Alberta  
Spring 1996



National Library  
of Canada

Acquisitions and  
Bibliographic Services Branch

395 Wellington Street  
Ottawa, Ontario  
K1A 0N4

Bibliothèque nationale  
du Canada

Direction des acquisitions et  
des services bibliographiques

395, rue Wellington  
Ottawa (Ontario)  
K1A 0N4

*Your file* *Votre référence*

*Our file* *Notre référence*

**The author has granted an irrevocable non-exclusive licence allowing the National Library of Canada to reproduce, loan, distribute or sell copies of his/her thesis by any means and in any form or format, making this thesis available to interested persons.**

**L'auteur a accordé une licence irrévocable et non exclusive permettant à la Bibliothèque nationale du Canada de reproduire, prêter, distribuer ou vendre des copies de sa thèse de quelque manière et sous quelque forme que ce soit pour mettre des exemplaires de cette thèse à la disposition des personnes intéressées.**

**The author retains ownership of the copyright in his/her thesis. Neither the thesis nor substantial extracts from it may be printed or otherwise reproduced without his/her permission.**

**L'auteur conserve la propriété du droit d'auteur qui protège sa thèse. Ni la thèse ni des extraits substantiels de celle-ci ne doivent être imprimés ou autrement reproduits sans son autorisation.**

ISBN 0-612-10747-7

**Canada**

UNIVERSITY OF ALBERTA

RELEASE FORM

NAME OF AUTHOR: Michael F. Polak

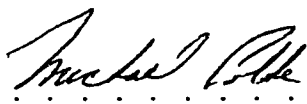
TITLE OF THESIS: **Quantifying Scoliotic Shape Using Surface Curvature**

DEGREE: Master of Science

YEAR THIS DEGREE GRANTED: 1996

Permission is hereby granted to the University of Alberta Library to reproduce single copies of this thesis and to lend or sell such copies for private, scholarly or scientific research purposes only.

The author reserves all other publication and other rights in association with the copyright in the thesis, and except as hereinbefore provided neither the thesis nor any substantial portion thereof may be printed or otherwise reproduced in any material form whatever without the author's prior written permission.

(Signed) . . .  . . . . .  
Michael F. Polak  
6811 - 112 A Street  
Edmonton, Alberta  
Canada, T6H 3K5

Date: *Jan. 23, 1996.*

UNIVERSITY OF ALBERTA

FACULTY OF GRADUATE STUDIES AND RESEARCH

The undersigned certify that they have read, and recommend to the Faculty of Graduate Studies and Research for acceptance, a thesis entitled **Quantifying Scoliotic Shape Using Surface Curvature** submitted by Michael P. Polak in partial fulfillment of the requirements for the degree of Master of Science.

*N. S. L. Durdle* .....  
Dr. Nelson Durdle (Supervisor)

*Z. Koles* .....  
Dr. Z. Koles

*Jack Mowchenko* .....  
Dr. J. Mowchenko

*J. Raso* .....  
J. Raso

Date: *Dec. 11, 1996* . . . . .

To my family for their encouragement and in memory of my grandfather, Earl  
Stanley Gardiner.

## **ABSTRACT**

Scoliosis is characterized by an abnormal curvature of the spine. In order to evaluate the progression of scoliosis or any potential treatment of it, a method of measuring the severity of the deformity is needed. Digital representations of the back surfaces of scoliosis patients are created using a stereo camera system. This data is transformed into a regularized depth field (a *Monge patch*) for analysis. This thesis presents an evaluation technique based on shape analysis. Shape representations are first constructed to segment the back surface into subsets of homogeneous regions. These shape regions are then quantized into single values through several different schemes. It is these final values that can be used to compare the changes to a surface over time as caused by deformity or the effects due to treatment. The measurements meet the requirements that they be invariant to changes in rotation, translation and scaling of the surface.

## **ACKNOWLEDGEMENTS**

Thanks to my fellow graduates in the lab who listened to my problems and offered advice - especially Ketan Bhalla and Roland Penner. Also I'd like to thank my brother for keeping me active outside of my studies with football and Dr. Margaret Ackman, Mark Polak, and Nelson Poon for the stress relief they provided with our weekly badminton games.



# TABLE OF CONTENTS

<b>1</b>	<b>Introduction</b>	<b>1</b>
1.1	Description of scoliosis . . . . .	1
1.2	Clinical application . . . . .	2
1.3	Objective . . . . .	5
1.4	Overview . . . . .	5
<b>2</b>	<b>Literature Review</b>	<b>7</b>
2.1	Measuring Spinal Deformity . . . . .	7
2.2	Shape analysis . . . . .	8
2.3	Discrete derivative calculation . . . . .	9
2.4	Quantifying change . . . . .	10
2.5	Summary . . . . .	11
<b>3</b>	<b>Curvature</b>	<b>12</b>
3.1	Theory . . . . .	12
3.1.1	Definition . . . . .	12
3.1.2	First fundamental form . . . . .	14

3.1.3	Second fundamental form . . . . .	15
3.1.4	Principal curvatures . . . . .	16
3.2	Discrete derivatives . . . . .	18
3.3	Discrete Approximation . . . . .	20
3.3.1	Differential Derivatives . . . . .	21
3.3.2	Scale-space . . . . .	24
3.4	Implementation . . . . .	28
3.4.1	Differential Derivative . . . . .	28
3.4.2	Gaussian Kernel . . . . .	29
<b>4</b>	<b>Shape Representation</b>	<b>40</b>
4.1	Defining shape . . . . .	40
4.2	Principal Curvatures . . . . .	42
4.3	Gaussian and mean curvature . . . . .	43
4.4	Shape Index . . . . .	46
4.5	Other classifications . . . . .	51
4.5.1	Ridge and Groove . . . . .	51
4.5.2	Gaussian feature points . . . . .	51
4.6	Summary . . . . .	52
<b>5</b>	<b>Applying shape analysis</b>	<b>53</b>
5.1	Obtaining information from shape regions . . . . .	53
5.1.1	Estimated surface area . . . . .	54

5.1.2	Projected surface area . . . . .	54
5.1.3	Principal Curvatures . . . . .	54
5.2	Accounting for size . . . . .	54
5.3	Determining equality . . . . .	56
<b>6</b>	<b>Experimental results</b>	<b>57</b>
6.1	Which kernel to use? . . . . .	57
6.2	Visual assessment of shape classifications . . . . .	59
6.3	Testing . . . . .	63
6.4	Rotation invariance . . . . .	64
6.4.1	Surface area . . . . .	64
6.4.2	Principal curvature directions . . . . .	66
6.4.3	Curvedness . . . . .	67
6.5	Scale invariance . . . . .	69
6.5.1	Surface area . . . . .	69
6.5.2	Principal curvature directions . . . . .	70
6.5.3	Curvedness . . . . .	70
6.6	Gaussian width effects . . . . .	71
6.6.1	Surface area . . . . .	72
6.6.2	Principal curvatures . . . . .	72
6.6.3	Curvedness . . . . .	73
6.6.4	Shape classification . . . . .	74

<b>7</b>	<b>Conclusions</b>	<b>76</b>
<b>8</b>	<b>Future Work</b>	<b>78</b>
	<b>Bibliography</b>	<b>80</b>
	<b>APPENDICES:</b>	<b>87</b>
<b>1</b>	<b>Vector Mathematics</b>	<b>87</b>
1.1	Vector Definition . . . . .	87
1.2	Vector Operations . . . . .	87
<b>2</b>	<b>Discrete Convolution</b>	<b>89</b>
<b>3</b>	<b>Discrete derivative kernels</b>	<b>91</b>

## LIST OF FIGURES

3.1	Tangent plane . . . . .	15
3.2	Sampled back surface . . . . .	19
3.3	3 x 3 neighbourhood of a surface point $(y_{u,v})$ . . . . .	23
3.4	Kernel coordinate reference frame . . . . .	28
3.5	Volume difference by kernel size (n x n) and Gaussian width (sigma) as compared with the theoretical volume of 1.0 . . . . .	32
3.6	A one-dimensional Gaussian with $\sigma = 1.0$ . . . . .	34
3.7	First derivative of $x^3 + 5x^2 + 12$ ( $3x^2 + 10x$ ) compared with Gaussian approximations . . . . .	36
3.8	Second derivative of $x^3 + 5x^2 + 12$ compared with Gaussian approximations	37
3.9	Second derivative approximation using two convolutions . . . . .	39
4.1	Example of shape representations . . . . .	42
4.2	Principal curvatures and directions of a scoliotic back surface . . . . .	44
4.3	Gaussian (left) and mean (right) curvature . . . . .	45
4.4	Curvature parameter plane . . . . .	46
4.5	Koenderink's shape space plane . . . . .	48

4.6	Shape classifications according to shape index scale . . . . .	50
6.1	$\delta f$ approx. using directional derivative . . . . .	58
6.2	$\delta^2 f$ approx. using directional derivative . . . . .	58
6.3	Shape classification colour legend . . . . .	60
6.4	Shape classifications using directional derivatives . . . . .	61
6.5	Shape classifications using Gaussian derivatives . . . . .	61
6.6	Shape classifications using direction derivatives . . . . .	62
6.7	Shape classifications using Gaussian derivatives . . . . .	62
6.8	Maximum curvature angle compared to cylinder rotation angle . . . .	67
6.9	Minimum curvature angle compared to cylinder rotation angle . . . .	67
6.10	Curvedness vs. $x$ rotation . . . . .	68
6.11	Normalized surface area as affected by scale changes . . . . .	69
6.12	Maximum curvature angle as affected by scale changes . . . . .	70
6.13	Minimum curvature angle as affected by scale changes . . . . .	71
6.14	Gaussian width effects on estimated surface area . . . . .	72
6.15	Sigma affect on rotated/non-rotated cylindrical surface areas . . . . .	73
6.16	Sigma affect on maximum curvature angle . . . . .	74
6.17	Sigma affect on minimum curvature angle . . . . .	74
6.18	Gaussian width effects on shape classification . . . . .	75

**LIST OF TABLES**

3.1 Sampled vs. Block averaged discrete Gaussian kernels . . . . . 33

4.1 Classifying Surface Types Using Principal Curvature Information . . . 42

4.2 Classifying Surface Types Using Gaussian and Mean Curvature Infor-  
mation . . . . . 46

4.3 Classifying Surface Types Using Shape Index . . . . . 50

6.1 Approximated surface area vs. z rotation . . . . . 65

6.2 Approximated surface area vs. x rotation . . . . . 65

6.3 Curvedness vs. z rotation . . . . . 68

6.4 Curvedness vs. cylinder radius . . . . . 71

# Chapter 1

## Introduction

### 1.1 Description of scoliosis

The goal of this work was to provide a means by which clinical technicians could monitor the progress of patients afflicted with scoliosis. In order to understand the requirements of a system which could achieve this goal, an understanding of the disease itself is needed.

Scoliosis is a spinal deformity that mostly affects otherwise healthy adolescent females. The abnormal curvature of the spine is usually coupled with axial rotation of the vertebra. Visible characteristics of the deformity usually include asymmetrical elevations of the shoulders and hips, a twisting of the trunk and a prominence of one of the shoulder blades. Treatment for scoliosis can vary from exercise therapy to corrective braces to surgery in the extreme cases. Early detection of scoliosis is desirable since treatment can help to prevent the possible deterioration of the spine and the need for surgical intervention. Scoliosis is most often detected in adolescent



females when they are going through a rapid growth spurt. For those that have been diagnosed as having scoliosis, progress is monitored by examining the patient's back postures and by examining x-ray representations of the spine. If the spinal curvature is worsening, alternate treatments are prescribed. The Scoliosis Research Society has specified curvature angles for use as references when prescribing treatment:

- $<20^\circ$ , normal spinal variation; treatment not required
- $>20^\circ$  and  $<50^\circ$ , non-surgical treatment required
- $>50^\circ$ , surgical correction required

Generally, treatment is not indicated unless the child is at a very high risk of progression and the curve is higher than  $25^\circ$ . Research at the Glenrose Rehabilitation Hospital has focused on a non-invasive measurement of the back as a possible alternative to frequent spinal x-ray analysis.

## 1.2 Clinical application

To evaluate the progression of scoliosis or any treatment of it, a characterization of the back surface is needed. Any proposed method to obtain this information should be non-invasive, repeatable, practicable, and accurate. The technique used at the Glenrose hospital entails acquiring a digital image of the scoliotic back through the use of two CCD television cameras [28]. The images from the two cameras are correlated to provide perspective information and consequently depth. The three-dimensional data is then reconstructed into a representation of the back surface [31].

The usefulness of this data as a means by which the scoliosis can be monitored depends on how it is evaluated.

The raw data obtained from the measuring instrumentation will in most cases be expressed relative to some arbitrary point. To aid in interpretation, a transformation to an alternate frame of reference may be performed. The problem with using an external reference frame for describing the data is that patient posture and position become a primary factor to the reproducibility of the data. Attempts have been made to standardize the patient posture so as to minimize positional variations [41]. Also, the addition of positional guides to standardize posture have been used. The influence that these positioning constraints exert on the patient's natural posture may hinder the examination of the abnormal spinal curvature. Since reproducibility is desired, the characterization method should avoid using an absolute reference coordinate frame and should attempt to base measurements on local changes and relative values. A measure of invariant characteristics is needed. Invariant characteristics are those attributes of a surface which do not vary with arbitrary changes in parameterization, translation, or rotation. The shape and scale of a surface are invariant characteristics that can be used to uniquely describe a surface. Since patient growth is another factor to be considered when attempting to monitor scoliosis by examining back surfaces, the size of the patient must be accommodated to allow for comparisons. Given this need to be scale independent, only the shape property of a surface can be used as the required invariant characteristic.

Asymmetry and complexity of back shape in scoliosis prevent a simple character-

ization by a few parameters. One rather has to study the whole back surface and take into account a variety of different structures. Both ISIS [38] and AUSCAN [32] quantify the curvature of the back in terms of various angles, displacements and distances. Surface shape is, however, weakly related to the internal spinal alignment [23]. A person may have considerable surface deformity with a relatively mild curvature of the spine while another person may have mild asymmetry of the trunk with a large spinal curvature. Change in either the internal spinal alignment or surface deformity is of particular concern as one may either lead or lag the other. Attempts to relate surface shape to spinal orientation will not be done in this work. Presently, qualitative analysis of a scoliotic back can be performed by viewing the re-constructed back surface. The goal of this work is to provide quantitative measures by which the scoliosis can be monitored. These quantitative results will be determined by segmenting the back into a few homogenous regions that share a similar shape. Each shape region will have parameters which can be used to monitor changes to the region.

The shape of a surface can be expressed mathematically as a function of surface curvature. Surface curvature has the benefit of being independent of coordinate representation and thus is not susceptible to an ill-defined reference frame. The use of surface curvature information has been used as a tool for scoliosis assessment by Frobin, Hierholzer and Drerup [40]. However, their use was strictly limited to a qualitative observation of the curvature segmented back image.

### 1.3 Objective

The goal of this research was to provide various measures to aid in the determination of the amount of change that has occurred on a uniformly sampled range data set. Since surface data of scoliotic trunks could be acquired at clinics at the Glenrose Hospital, the system was designed to satisfy three clinical constraints. The developed system must be sensitive enough to detect clinically relevant changes in shape and be easy to interpret. The measuring techniques must be robust so that changes in the orientation of the patient during data acquisition does not significantly affect the resultant information. Also, the analysis of the back surface changes should not be affected by possible growth of the patient between visits.

### 1.4 Overview

Chapter 2 contains a literature review on the work that has been done in areas applicable to this thesis. Chapter 3 presents the theory of curvature. Surface curvature is an important property and it is necessary to understand the mathematics upon which it is based since it is a fundamental part of the back shape analysis. Also discussed in this chapter are methods for determining curvature with a description of two techniques for determining the quantity using discrete data. The first technique is the directional derivative approach [40],[17],[13] and the second technique is the Gaussian convolution approach [44],[26],[25],[21] and [24]. Implementation considerations will then be analyzed to determine how to produce the best results. Chapter 4 presents

various techniques to represent shape using curvature information. Segmenting the back surface into smaller regions is then discussed as a means to simplify the analysis of the scoliotic deformity. In chapter 5 formulae are introduced to provide measurable parameters for the shape regions. The results of testing these formulae with data will be presented and then analyzed in chapter 6. The tests ensure that the clinical requirements of invariance to rotation and scaling are met. In chapter 7 a conclusion is given which comments on the results and summarizes the effectiveness of the different techniques used to produce the shape measurements. Future enhancements and areas for further research related to this thesis are provided in chapter 8.

# Chapter 2

## Literature Review

### 2.1 Measuring Spinal Deformity

There have been many attempts at finding clinically relevant measures of spinal deformity. Of the non-invasive techniques the most commonly mentioned are the ISIS [38],[22] and AUSCAN [32] systems. The ISIS system uses a projector to cast a plane of light onto a patient's back at specific vertical locations. These locations are manually marked on the back with adhesive markers prior to data collection. A camera transmits the view of each light plane to a computer for capture and storage. Each projected plane of light appears as a curved line from the camera's viewpoint. Together the lines produce a rough approximation of the back surface. Angles and distances are measured from the various curves to provide diagnostic information. The AUSCAN system captures the entire patient back surface with a single video image and then processes this image. Processing of the image consists of detecting the small, reflective, cylindrical adhesives which have been placed at various points on the

patient's back. These markers are usually placed in pairs so as to be able to measure the body symmetries. Measurements consist mostly of angles associated with these symmetry axes. Some of the problems associated with these systems are that the patient's posture must be controlled and there is an inherent error introduced with the manual placement of the reference markers and patient movement if more than one video frame is required. Also, since acquisition process is labor intensive, it is very time consuming.

Other researchers have tried to make the connection between features on the back and the underlying skeletal structure [4],[13],[33],[13],[19],[39],[17]. One of the measurements made by Stokes [19] was a tangential angle of the back surface at each vertebrae. Around the same time Drerup [4] examined tangential angles at the same points but from a lateral (side) view. Drerup found that the back profile angles related well to the same angular measurements taken from lateral x-rays. Since scoliosis can affect the back symmetry in more than one plane, Drerup used the curvature analysis method of Frobin [15] to examine the entire back surface. Drerup compared two range images of a scoliotic patient's back taken two years apart and concluded that the curvature maps showed great similarity. This use of curvature for back shape analysis prompted further study of the technique.

## **2.2 Shape analysis**

In the vision and image processing domain, shape analysis is a widely used technique for segmenting objects or features from their environment [37],[10],[16], [12],[20]. The

shape property is almost exclusively associated with the curvature of the surface being examined. Trucco [37] performed experiments to evaluate a range image segmentation system which partitioned range data into homogeneous surface patches based on the sign of the mean and Gaussian curvatures. Ittner [20] used a collection of six local curvature measures to classify three-dimensional objects from acquired range data. Goldgof, Huang and Lee [12] used the extreme values of Gaussian and mean curvatures to establish feature points for use in matching terrain data with a large geographical database. Besl and Jain [7, 8, 9, 10] have produced a number of papers relating to image segmentation based on curvature and on the techniques for the calculation of surface curvature. Curvature features have been used to recognize human faces [16] and of a more relevant nature, have been used to find anatomical landmarks on the human back [17], [13].

### **2.3 Discrete derivative calculation**

Since curvature maps will be used to help analyze back shape, a reliable method must be found to calculate the curvatures. Surface curvature depends on tangents to the surface at the point being examined. Tangents are related to partial derivatives of the surface equation. Therefore, finding a reliable method for calculating curvature is the same as finding a reliable method for calculating partial derivatives. Determining partial derivatives from parametric equations is explained by Stewart [35]. The back surface data collected by the data acquisition system at the Glenrose is a quantized representation of the true surface as is true for any range imaging system. The meth-



ods used for the calculation of the partial derivatives of the back surface must offer a discrete solution. Discrete curvature or partial derivative calculation methods are offered by Mitchell[30],Bennett[6], and Taratorin[36]. The previously mentioned papers find either the partial derivative or the particular curvature directly from the quantized data. Another way of finding the same information is through indirect means. The partial derivative information could be the result of an operation performed on the data. This is how derivative quantities are found in Florack[29],[27], and Romeny [5].

## 2.4 Quantifying change

There is minimal information on procedures used to quantify change based on shape classifications. Related areas of research in computer vision are primarily concerned with matching the analyzed image as a whole to some generalized version [9], [7]. Other researchers have used the curvature information to locate a set of feature points for matching operations. Features that have moved or changed are ignored and only those that have remained the same are used in the matching process [37],[16]. Besl [8] provides some quantities which may be of interest in surface characterization. Some of Besl's surface characterization quantities have been implemented as possible measures of change. In addition, Koenderink and van Doorn [26] describe a measure of scale called *curvedness* which they used to compensate for the effects of scale. Children are typically growing very rapidly during the observation period so it is necessary to accommodate growth.

## **2.5 Summary**

The shape analysis process developed in this work has made use of many of the research papers described previously. Curvature was used to quantify shape and also played a role in segmenting the surface so as to simplify the amount of information to analyze. Implementation proved to be the biggest challenge and in several instances required an adaptation of a formula or technique in order to achieve the desired result.

# Chapter 3

## Curvature

In order to quantify shape some mathematically obtainable value is needed which can be calculated from the data. Researchers studying vision have attributed curvature as a primary characteristic that provides information about shape [3][34]. A description of curvature and details about the implementation used to calculate curvature is discussed below.

### 3.1 Theory

#### 3.1.1 Definition

Curvature is a property that can only be measured in a plane. In order to discuss “surface curvature” we must establish a method by which a three-dimensional surface can be projected onto appropriate planes. Let us consider some surface defined in three dimensions that can be specified as the height above a plane. This type of representation is known as a *graph surface* representation and the surface itself is

called a *Monge patch* [8]. For any point on the surface we can determine a tangential vector by examining changes in height with respect to the reference plane. The change in height along the vector can be viewed as a curve in two dimensions. The curvature of the surface for that direction is the “bending” of this space curve away from its tangent plane with the magnitude being measured by the radius of a circle that best approximates the “bend”. If two vectors are chosen such that one of the curves has the maximum radius and the other has the minimum radius, then the curvatures are known as the *principal curvatures* with the directions of the vectors being appropriately named the *principal directions* [2].

Let  $\vec{\mathbf{r}}(u, v)$  represent a regular surface defined parametrically in three dimensions.

$$\vec{\mathbf{r}}(u, v) = (x(u, v), y(u, v), z(u, v)) \quad (3.1)$$

where  $\vec{\mathbf{r}}$  is the vector from the origin of an arbitrary 3D coordinate system to the sampled point;  $x$ ,  $y$ , and  $z$  are its 3D coordinates; and  $(u, v)$  are the parameters of the 2D space in which the data is mapped. The graph surface is assumed to be smooth and be at least twice differentiable<sup>1</sup>. Given such a surface, two basic equations, known as the *first fundamental form* and the *second fundamental form* [2], have been used to define many surface properties.

---

<sup>1</sup>A function  $f$  is **differentiable at a** if  $f'(a)$  exists for all values of  $a$ . To be **twice differentiable** requires that  $f''(a)$  exist as well.

### 3.1.2 First fundamental form

The first fundamental form is one of two equations well established in the subject of differential geometry. The definition of the first fundamental form, denoted by the roman numeral  $I$ , is

$$I(u, v, du, dv) = d\vec{\mathbf{r}} \cdot d\vec{\mathbf{r}} \quad (3.2)$$

$$= E du^2 + 2F du dv + G dv^2 \quad (3.3)$$

where

$$E = \vec{\mathbf{r}}_u \cdot \vec{\mathbf{r}}_u \quad (3.4)$$

$$F = \vec{\mathbf{r}}_u \cdot \vec{\mathbf{r}}_v \quad (3.5)$$

$$G = \vec{\mathbf{r}}_v \cdot \vec{\mathbf{r}}_v \quad (3.6)$$

$$\vec{\mathbf{r}}_v(u, v) = \partial \vec{\mathbf{r}} / \partial v \quad (3.7)$$

$$\vec{\mathbf{r}}_u(u, v) = \partial \vec{\mathbf{r}} / \partial u \quad (3.8)$$

The first fundamental form will not be used directly but the coefficients  $E$ ,  $F$ , and  $G$  are used in the determination of surface curvature.

The two linearly independent tangents to the surface,  $\vec{\mathbf{r}}_u$  and  $\vec{\mathbf{r}}_v$  define a plane known as the *tangent plane* (see figure 3.1). All tangents to the parameter curves on the surface at a point  $(u, v)$  lie on this plane. Because  $I(u, v, du, dv)$  is invariant to the rotation, the translation, and the parameterization of the surface, it is said that the first fundamental form is an *intrinsic* surface property. Intrinsic properties are

significant since the same intrinsic surface primitive viewed from two distinct viewpoints remains the same for each viewpoint. This property is key to our assessment of possible back shape parameters since the viewpoint of the cameras may be not always be the same with respect to the patient. *Extrinsic* properties, on the other hand, depend on how the surface is embedded in the 3D space and will be different for the two viewpoints [18]. The functions  $E, F,$  and  $G$  are also invariant with respect to coordinate transformations .

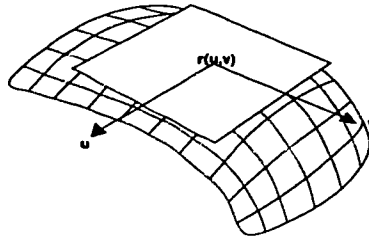


Figure 3.1: Tangent plane

### 3.1.3 Second fundamental form

The second fundamental form is another equation well established in the subject of differential geometry. The definition of the second fundamental form, denoted by the roman numeral  $II$ , is

$$II(u, v, du, dv) = -d \vec{\mathbf{r}} \cdot d \vec{\mathbf{n}} \quad (3.9)$$

$$II(u, v, du, dv) = L du^2 + 2 M du dv + N dv^2 \quad (3.10)$$

where

$$\vec{\mathbf{n}} = \frac{\vec{\mathbf{r}}_u \times \vec{\mathbf{r}}_v}{\| \vec{\mathbf{r}}_u \times \vec{\mathbf{r}}_v \|} \quad (3.11)$$

$$L = \vec{\mathbf{r}}_{uu} \cdot \vec{\mathbf{n}} \quad (3.12)$$

$$M = \vec{\mathbf{r}}_{uv} \cdot \vec{\mathbf{n}} \quad (3.13)$$

$$N = \vec{\mathbf{r}}_{vv} \cdot \vec{\mathbf{n}} \quad (3.14)$$

$$\vec{\mathbf{r}}_{vv}(u, v) = \partial^2 \vec{\mathbf{r}} / \partial v^2 \quad (3.15)$$

$$\vec{\mathbf{r}}_{uu}(u, v) = \partial^2 \vec{\mathbf{r}} / \partial u^2 \quad (3.16)$$

$$\vec{\mathbf{r}}_{uv}(u, v) = \partial^2 \vec{\mathbf{r}} / \partial v \partial u. \quad (3.17)$$

The vector  $\vec{\mathbf{n}}$  is known as the *surface normal vector* and is perpendicular to the tangent plane. Combined with the two unnormalized vectors  $\vec{\mathbf{r}}_u$  and  $\vec{\mathbf{r}}_v$ ,  $\vec{\mathbf{n}}$  forms a local coordinate system at the point  $\vec{\mathbf{r}}(u, v)$ . As with the first fundamental form,  $I(u, v, du, dv)$ , the second fundamental form will not be used directly, but the coefficients that arise from its derivation will be used -  $L$ ,  $M$ ,  $N$ .

Perhaps the most important surface property for our purposes is curvature,  $\kappa$ . Of particular interest are the principal curvatures,  $\kappa_1$  and  $\kappa_2$ , referred to also as the maximum curvature and the minimum curvature, respectively. By using the coefficients from the first and second fundamental forms the principal curvatures can be defined.

### 3.1.4 Principal curvatures

Surface curvature was previously described as relating to the radius of a circle that best approximated the “bending” of a space curve away from the tangential plane. The principal curvatures are associated with the maximum and minimum radii that

can be found for a given point on a surface. The principal curvatures,  $\kappa_1$  and  $\kappa_2$ , may be calculated by solving

$$\det \begin{bmatrix} \kappa E - L & \kappa F - M \\ \kappa F - M & \kappa G - N \end{bmatrix} = 0 \quad (3.18)$$

which will generally result in two solutions. The larger value is known as the maximum curvature,  $\kappa_1$ , and the smaller value is known as the minimum curvature,  $\kappa_2$ . E, F, G, L, M, and N are the coefficients from the first and second fundamental forms and are defined in equations 3.4, 3.5, 3.6, 3.12, 3.13, and 3.14 respectively. The directions, in the parameter plane, of the maximum and minimum  $\kappa$  are referred to as the principal directions. The principal directions are given by the angles derived from the roots of

$$\det \begin{bmatrix} \tau^2 & -\tau & 1 \\ E & F & G \\ L & M & N \end{bmatrix} = 0 \quad (3.19)$$

where  $\tau = du/dv = \tan\theta$ , and  $\theta$  is the angle in the parameter  $(u,v)$ -plane. Using  $\kappa_1$  and  $\kappa_2$ , Gaussian K and mean H curvature values may also be defined:

$$K = \kappa_1 \kappa_2 = \frac{LN - M^2}{EG - F^2} \quad (3.20)$$

$$H = \frac{1}{2}(\kappa_1 + \kappa_2) = \frac{EN + GL - 2FM}{2(EG - F^2)}. \quad (3.21)$$

The Gaussian curvature is an important quantity since it can represent the surface curvature with a single number and is invariant to all rigid geometrical transformations. Due to its averaging nature, mean curvature is less susceptible to noise as compared to Gaussian curvature. Mean curvature, however, is an extrinsic surface property whereas Gaussian curvature is an intrinsic property.



Given a continuous, twice differentiable graph surface, the surface curvature can be found. A problem arises, however, when the graph surface is not continuous but discrete as is the case of trunk image data. The calculation of accurate discrete partial derivatives is a topic that is still being researched [36],[42].

### **3.2 Discrete derivatives**

A stereo pair of CCD television cameras is used to obtain the depth maps of scoliotic patient back surfaces. The acquisition process begins by first projecting a known pattern of horizontal lines of varying thickness onto the patient's back. Images are captured from two cameras and the lines in the two images are matched. Geometric information from the cameras and the line positions is used to establish the depth of points on each line [28]. This coordinate information is stored in a text file. A separate graphical viewing program [31] facilitates viewing the calculated back surface under controlled lighting conditions and surface textures. Penner [31] has also added the ability to resample the irregular three dimensional surface coordinate data into a regularized grid of any desired density. It is this regularized grid surface data that is used for back shape analysis. Figure 3.2 shows a regular grid-sampled back surface viewed with this program. For shape analysis it will be necessary to determine various partial derivatives of this discrete surface. The following sections will describe the implementation of the two techniques for approximating the partial derivatives of a discretely sampled surface.

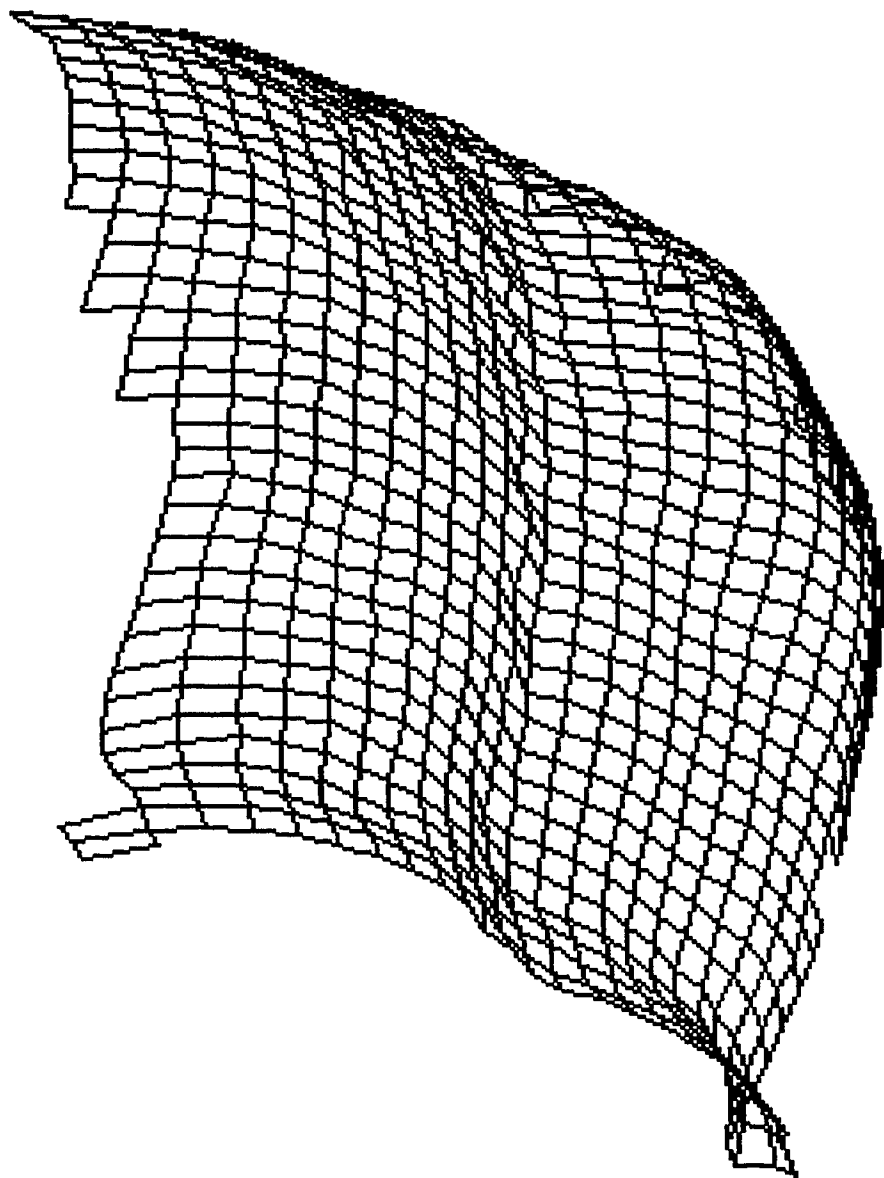


Figure 3.2: Sampled back surface

### 3.3 Discrete Approximation

Discrete approximations of curvature are susceptible to both image noise and quantization limitations [14]. The higher the order of the derivative to be approximated, the greater the influence of high frequency image components - noise in particular. Typically, smoothing of the image is performed beforehand to remove the higher frequencies. In cases where edge information is important, smoothing can cause the loss of valuable information.

Approximation methods can be divided into two primary categories: fitting data points to a curve or applying kernel operators. To obtain the necessary partial derivatives, the first technique attempts to find the equation of a curve that best fits the data and then calculates the required derivatives based on the curve function [10]. Fitting variable-order surfaces to our data is not recommended as the piece-wise surface approximations require sufficiently large regions (10-30 points) that can not be guaranteed since the size of a region is only determined by its shape attribute. Also, choosing the order of polynomial to fit to the data can be difficult. A low order polynomial may not adequately capture the sharp changes of a prominent shoulder blade for instance while a higher order polynomial may create an irregular fit due to noise on a flat region. The other possible method for approximating partial derivatives involves kernel operators. The kernel method consists of convolving a square matrix with a rectangular grid sampled (*raster*) data set. The values placed in the matrix are specific to the operation to be performed, but in the simplest case consists of quantities based on differential methods and on the theory of the directional derivative.

Only the kernel operator method was implemented in this work. The primary reason for this choice was that the majority of the methods used for shape analysis assumed both regularized data and kernel operations.

In order to find the curvature at a point on a surface, tangents to the surface at that point are required. These tangential lines are found by determining the partial derivatives of the surface function. Since the patient data being analyzed is discrete, approximations are needed as there is no known surface function. The kernel operator method establishes a set of discrete points on which an operation will be performed. If the kernel contains elements which approximate a partial derivative operation, the affect of convolving the kernel with a local region of data points will be an approximation to the partial derivative at the center point of the region. Two methods for selecting values for the kernel matrix will be examined: the differential derivative approach and the scale-space approach.

### 3.3.1 Differential Derivatives

For a continuous function, a derivative in a particular direction requires evaluating the difference between two points an infinitesimal distance apart. The convention for determining partial derivatives for a raster image requires approximating the infinitesimal distance by the neighbouring data points. The data points are typically calls pixels when the data set represents an image. This approximation technique arises from the direct interpretation of the directional derivative. For a surface  $r$  defined parametrically in terms of a  $u$  and  $v$  coordinate axis the **directional derivative** of

$\vec{\mathbf{r}}$  at  $(u_0, v_0, r(u_0, v_0))$  is

$$D_u \vec{\mathbf{r}}(u_0, v_0) = \lim_{h \rightarrow 0} \frac{r(u_0 + hu, v_0 + hb) - r(u_0, v_0)}{h}$$

where in the context of raster images,  $h$  is the raster period. The displacements along the  $u$  and  $v$  axes could potentially be any integer value but for our purposes  $a$  and  $b$  will only have the values of either 0 or 1. The complete directional derivative in the  $u$  (horizontal) direction is composed from both the  $u^+$  and  $u^-$  directions. For all directions along the  $u$  axis,  $b$  is 0. Also, since the neighbourhood approximation will only consist of the immediately adjacent pixel,  $a$  will be 1.  $r_{u+}$  represents an approximation of the horizontal slope in the  $u^+$  direction.  $r_{u-}$  represents an approximation of the horizontal slope in the  $u^-$  direction. Together, the two results provide an overall approximation to the horizontal slope at the center of the local neighbourhood being examined.

$$\begin{aligned} r_{u+}(u, v) &= \lim_{h \rightarrow 0} \frac{r(u_0 + h, v_0) - r(u_0, v_0)}{h} \\ r_{u-}(u, v) &= \lim_{h \rightarrow 0} \frac{r(u_0 - h, v_0) - r(u_0, v_0)}{h} \\ r_u(u, v) &= r_{u+}(u, v) - r_{u-}(u, v) \\ r_u(u, v) &= \lim_{h \rightarrow 0} \frac{r(u_0 + h, v_0) - r(u_0 - h, v_0)}{h} \end{aligned} \quad (3.22)$$

Let  $\mathbf{g}_{u,v}$  represent the immediate neighbouring pixels in the 3 x 3 neighbourhood as shown in figure 3.3. The value at each of the nine discrete locations in the neighbourhood is obtained from the surface data which is height (or depth) information. An approximation to  $\vec{\mathbf{r}}_u$ ,  $\Delta \vec{\mathbf{r}}_u$ , can then be expressed as:

$$\Delta \vec{\mathbf{r}}_u(u, v) = \langle 2h, 0, g_{1,0} - g_{-1,0} \rangle$$

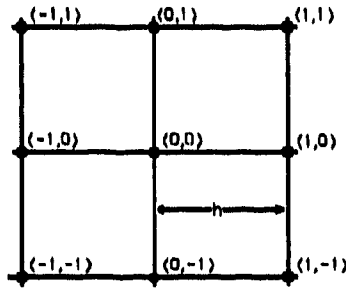


Figure 3.3: 3 x 3 neighbourhood of a surface point  $(g_{u,v})$ .

The magnitude of the vector components of  $\Delta \vec{\mathbf{r}}_u(u, v)$  can be normalized by dividing each term by  $2h$ . This results in the simplified form:

$$\Delta \vec{\mathbf{r}}_u(u, v) = \left\langle 1, 0, \frac{g_{1,0} - g_{-1,0}}{2h} \right\rangle \quad (3.23)$$

The remaining derivatives can be obtained in a similar manner as shown in Abramowitz [1] (see appendix 3 for a more complete derivation). Frobin and Hierholzer produce comparable results although their method attempts to improve the kernels' susceptibility to noise by averaging more of the neighbourhood points into the equations as in equations 3.24 to 3.28. For approximating the partial derivative in the  $u$  direction equation 5.1 only used the two outside points of the middle row of the neighbourhood matrix. Frobin and Hierholzer used the outside points of all three rows and thus could average the result over six points as opposed to just two.

$$\Delta \vec{\mathbf{r}}_u(u, v) = \left\langle 1, 0, \frac{g_{1,1} - g_{-1,1} + g_{1,0} - g_{-1,0} + g_{1,-1} - g_{-1,-1}}{6h} \right\rangle \quad (3.24)$$

$$\Delta \vec{\mathbf{r}}_v(u, v) = \left\langle 0, 1, \frac{g_{-1,1} - g_{-1,-1} + g_{0,1} - g_{0,-1} + g_{1,1} - g_{1,-1}}{6h} \right\rangle \quad (3.25)$$

$$\Delta \vec{\mathbf{r}}_{uv}(u, v) = \left\langle 0, 0, \frac{g_{1,1} - g_{-1,1} + g_{-1,-1} - g_{1,-1}}{4h} \right\rangle \quad (3.26)$$

$$\Delta \vec{\mathbf{r}}_{uu}(u, v) = \langle 0, 0, \frac{g_{1,0} + g_{-1,0} + g_{1,1} + g_{-1,1} + g_{1,-1} + g_{-1,-1} - 2(g_{0,0} + g_{0,1} + g_{0,-1})}{3h^2} \rangle \quad (3.27)$$

$$\Delta \vec{\mathbf{r}}_{vv}(u, v) = \langle 0, 0, \frac{g_{0,1} + g_{0,-1} + g_{1,1} + g_{1,-1} + g_{-1,1} + g_{-1,-1} - 2(g_{0,0} + g_{1,0} + g_{-1,0})}{3h^2} \rangle \quad (3.28)$$

The above equations were implemented as one method to approximate partial derivatives for a discrete surface. Another technique used to obtain the same information is associated with a concept known as scale-space.

### 3.3.2 Scale-space

The second technique used to approximate partial derivatives of a discretely sampled surface was found in computer vision research literature. A common approach to the analysis of digitized images is to use the Fourier transform to examine the frequency spectrum of the data. A similar analysis can be done in the spatial domain with a different operation. By convolving the image with a special scalable function the image can be viewed at multiple scales - similar to examining a breakdown by frequency composition. The transformation of the image data in this manner produces a scale-space version of the image.

Florack [29] discussed the benefits of scale-space image analysis and provided a persuasive argument against the use of neighbouring pixel approximations - a key assumption in the differential derivative approach discussed previously. Florack referred to the use of neighbouring pixels to approximate infinitesimal distances as a *“non-robust and rather ad-hoc solution that crucially relies on imaging conditions,*

*like grid size and pixel shape*". Using kernels based on the pixel-neighbourhood convention implies that the structures of interest in the image have a spatial extent close to pixel scale. Since this is not generally the case, it makes no sense to use this type of approximation. Florack presented a complete hierarchy of scaled differential operators which do not make assumptions on the scale of possible regions of interest in an image. Florack described the attributes of a scale-space operator for a front-end vision system and derived it mathematically. Florack reached the same conclusions as Babaud [21] who earlier presented a mathematically based argument for the uniqueness of the Gaussian as a scale-space kernel operator.

The "blurring" of an image caused by the change of scale of the scale-space operator is reminiscent of a filter operation and in fact behaves as such. The scale of the operator performs a similar function to the bandwidth of a low-pass filter but in a reciprocal manner. For small values of the scale parameter almost all of the frequencies that exist in the image being operated on are present. As the scale parameter is increased the higher frequencies are "filtered" out and the visual effect is that the image becomes "blurred" - the result of seeing only the less detailed lower frequency components of the image. Mathematical proofs derived by Babaud [21] and other mathematical justifications by Florack [29] formed the foundation for the acceptance of the Gaussian as the unique scale-space kernel operator. Babaud began his proof by listing the attributes that the ideal kernel operator must have and then proceeded to find a function that meets all these criteria. These criteria are:

- the scale parameter influences the kernel by stretching it along an axis while



keeping its area invariant

- the kernel is symmetric ( thus even and not causal )
- the kernel has unit area
- the kernel is infinitely differentiable

Florack's proposed requirements for a front-end vision system are:

- *linearity*: allowing for superposition of input stimuli
- *spatial shift invariance*: implied by the absence of a preferred location
- *isotropy*: implied by the absence of a preferred direction
- *scale invariance*: implied by the absence of a preferred scale

Florack concluded that the constraints arising from the lack of *a priori* geometrical knowledge lead to the choice of the Gaussian kernel and its derivatives as the most suitable scale-space operators for the study of image structure.

The important concepts introduced by scale-space analysis as they pertain to this work are: 1) no assumptions are made about data sampling, 2) an operator is provided that is not susceptible to data orientation or scale, and 3) derivatives of the Gaussian operator maintain the same attributes as the Gaussian operator.

To produce a scale-space image at a particular scale, a normalized Gaussian kernel is convolved with the image, the width of which corresponds to the inner scale (  $\sigma$  ). The Gaussian function has a number of important properties described above that

make it suitable for the role of the scale-space operator. Expressed in an alternate manner these properties are: absence of spurious detail, linearity, and invariance to translation, rotation and scale. The problem of finding derivatives that depend continuously on the image has a trivial solution given a smooth scale-space kernel. Letting  $\mathcal{D}$  represent any linear differential operator,  $i$  represent the image to be analyzed, and  $g_\sigma$  represent the scale-space kernel on a scale  $\sigma$ , then the convolution of  $i * \mathcal{D}g_\sigma$  precisely yields the desired derivative. The complete definition of this theorem is given in equation 3.29. The effect of varying  $\sigma$  on shape analysis will be discussed later. The concepts introduced by scale-space analysis provide an alternate means for finding partial derivatives of a surface that are necessary for curvature calculations. At the same time, the scale parameter of the Gaussian kernel operator can be used to control the contribution of surrounding data to the evaluation of the partial derivatives.

$$\mathcal{D}\{i * g_\sigma\} = \mathcal{D}i * g_\sigma = i * \mathcal{D}g_\sigma \quad (3.29)$$

The normalized two dimensional Gaussian can be expressed as:

$$g(x, y) = \frac{e^{-\frac{x^2+y^2}{2\sigma^2}}}{2\pi\sigma^2} \quad (3.30)$$

with the corresponding partial derivatives:

$$\frac{\partial g(x, y)}{\partial x} = \frac{-x e^{-\frac{x^2+y^2}{2\sigma^2}}}{2\pi\sigma^4} \quad (3.31)$$

$$\frac{\partial g(x, y)}{\partial y} = \frac{-y e^{-\frac{x^2+y^2}{2\sigma^2}}}{2\pi\sigma^4} \quad (3.32)$$

$$\frac{\partial^2 g(x, y)}{\partial x \partial y} = \left(\frac{xy}{\sigma^2}\right) \frac{e^{-\frac{x^2+y^2}{2\sigma^2}}}{2\pi\sigma^4} \quad (3.33)$$

$$\frac{\partial^2 g(x, y)}{\partial x^2} = \left(\frac{x^2}{\sigma^2} - 1\right) \frac{e^{-\frac{x^2+y^2}{2\sigma^2}}}{2\pi\sigma^4} \quad (3.34)$$

$$\frac{\partial^2 g(x, y)}{\partial y^2} = \left( \frac{y^2}{\sigma^2} - 1 \right) \frac{e^{-\frac{x^2+y^2}{2\sigma^2}}}{2\pi\sigma^4} \quad (3.35)$$

## 3.4 Implementation

Both the differential derivative method and the Gaussian convolution method for approximating partial derivatives were implemented. Details of the implementations are provided in the following sections.

### 3.4.1 Differential Derivative

Using the assumption that the an infinitesimal neighbourhood can be adequately approximated by a neighbouring pixel, a set of derivative kernels can be created. Using a 3 x 3 matrix, a coordinate system is defined such that the central location can be referenced as 0,0. This coordinate system is shown in figure 3.4.

$g_{-11}$	$g_{01}$	$g_{11}$
$g_{-10}$	$g_{00}$	$g_{10}$
$g_{-1-1}$	$g_{0-1}$	$g_{1-1}$

Figure 3.4: Kernel coordinate reference frame

By using equations 3.24 to 3.28 and the coordinate system shown above, a collection of first and second order partial derivative kernels can be constructed. These kernels are shown below:

$$\begin{array}{ccc}
 \vec{r}_u = \frac{1}{6h} \begin{array}{|c|c|c|} \hline -1 & 0 & 1 \\ \hline -1 & 0 & 1 \\ \hline -1 & 0 & 1 \\ \hline \end{array} & \vec{r}_v = \frac{1}{6h} \begin{array}{|c|c|c|} \hline 1 & 1 & 1 \\ \hline 0 & 0 & 0 \\ \hline -1 & -1 & -1 \\ \hline \end{array} & \vec{r}_{uu} = \frac{1}{3h^2} \begin{array}{|c|c|c|} \hline 1 & -2 & 1 \\ \hline 1 & -2 & 1 \\ \hline 1 & -2 & 1 \\ \hline \end{array} \\
 \\
 \vec{r}_{vv} = \frac{1}{3h^2} \begin{array}{|c|c|c|} \hline 1 & 1 & 1 \\ \hline -2 & -2 & -2 \\ \hline 1 & 1 & 1 \\ \hline \end{array} & \vec{r}_{uv} = \frac{1}{4h^2} \begin{array}{|c|c|c|} \hline -1 & 0 & 1 \\ \hline 0 & 0 & 0 \\ \hline 1 & 0 & -1 \\ \hline \end{array} & 
 \end{array}$$

The other method for producing partial derivative approximations using discrete data involves convolution with a Gaussian kernel operator.

### 3.4.2 Gaussian Kernel

To implement the discrete convolution of a Gaussian kernel with a raster image a kernel size must be chosen. The choice of kernel size is not arbitrary and can have a major effect on the quality of the derivative being sought. The choice of kernel size depends on the tolerance level for data loss due to edge effects, truncation problems fitting a discretely sampled Gaussian into the kernel, and computation time. Computation time becomes a problem when the kernel size becomes very large because there are a large number of computations for each resultant point. In this work computation time was not a concern since the other factors require the kernel size to be relatively small. For most tests a kernel size of  $7 \times 7$  was used.

### Kernel edge effects

Edge effects relate to the problem caused by lack of data points at the extreme ends of a data set involved in a discrete linear convolution operation. In the one-dimensional case, linear convolution on the data set  $x(n)$  with a function  $h(n)$  for  $0 \leq n \leq N - 1$  is defined as shown in equation 3.36.

$$y(n) = \sum_{k=0}^{N-1} h(k)x(n - k) \quad (3.36)$$

The size of the operator  $h(n)$  is  $N$  samples. Since  $x(n)$  only has values for  $0 \leq n \leq N - 1$ , there are no defined values when  $n - k < 0$ . This is the situation that causes edge effects. In some cases the undefined values can be assumed to be zero with no harmful effects but that is not usually the case when performing convolution with images. Since the convolution operation cannot be properly computed on these edge points, the standard solution is to only perform the convolution on points for which all the necessary data exists. This results in a loss of  $(N - 1)/2$  data points on each edge of the image (assuming that the operator kernel is of size  $N \times N$ ). The boundary data points of the sampled back surface are of lesser diagnostic value than the large proportion of points which compose the rest of the surface. Liu [28] explained the problems with determining boundary points for the back surface data.

### Gaussian kernel size

In addition to edge effects, there is another factor to consider when determining a suitable size for the kernel operator. The operator is to be a Gaussian function which has a scale parameter  $\sigma$ . The width of the Gaussian can be varied by changing the

magnitude of  $\sigma$ . For best convolution results, a kernel should have values at its edges that are zero. The continuous Gaussian function does approach zero at its outer limits but the edge values of the kernel depend on the size of  $\sigma$  and on the sampling method used. As the Gaussian width,  $\sigma$ , increases, the percentage of the function volume that is within the boundaries of the kernel decreases. The resulting kernel no longer has a smooth transition from the peak of the Gaussian to zero at the edges. Figure 3.5 shows how the volume of the two-dimensional Gaussian kernel is affected by both kernel size and the magnitude of  $\sigma$ . The volume differences compared in the chart are with respect to the volume of the continuous normalized Gaussian which is 1.0.

After choosing an appropriate kernel size, the kernel must be given values for each location within the matrix. Since the kernel has a limited number of entries, the continuous Gaussian must be sampled in order to obtain the needed values. The direct approach to obtaining samples of the continuous Gaussian would be to evaluate equation 3.30 at integer values  $[-N/2, N/2]$  corresponding to entry coordinates in the  $N \times N$  kernel. For larger values of  $\sigma$  there are no great inaccuracies in the resulting convolution operation provided the kernel is large enough to avoid truncation effects. However, for  $\sigma$  values close to  $N/2$ , the resulting convolution can be very incorrect due to poor approximation of the Gaussian volume. An alternate method to direct sampling of the Gaussian is to obtain two samples near the point determined by the direct sampling method and average them; this is known as *block sampling*. The

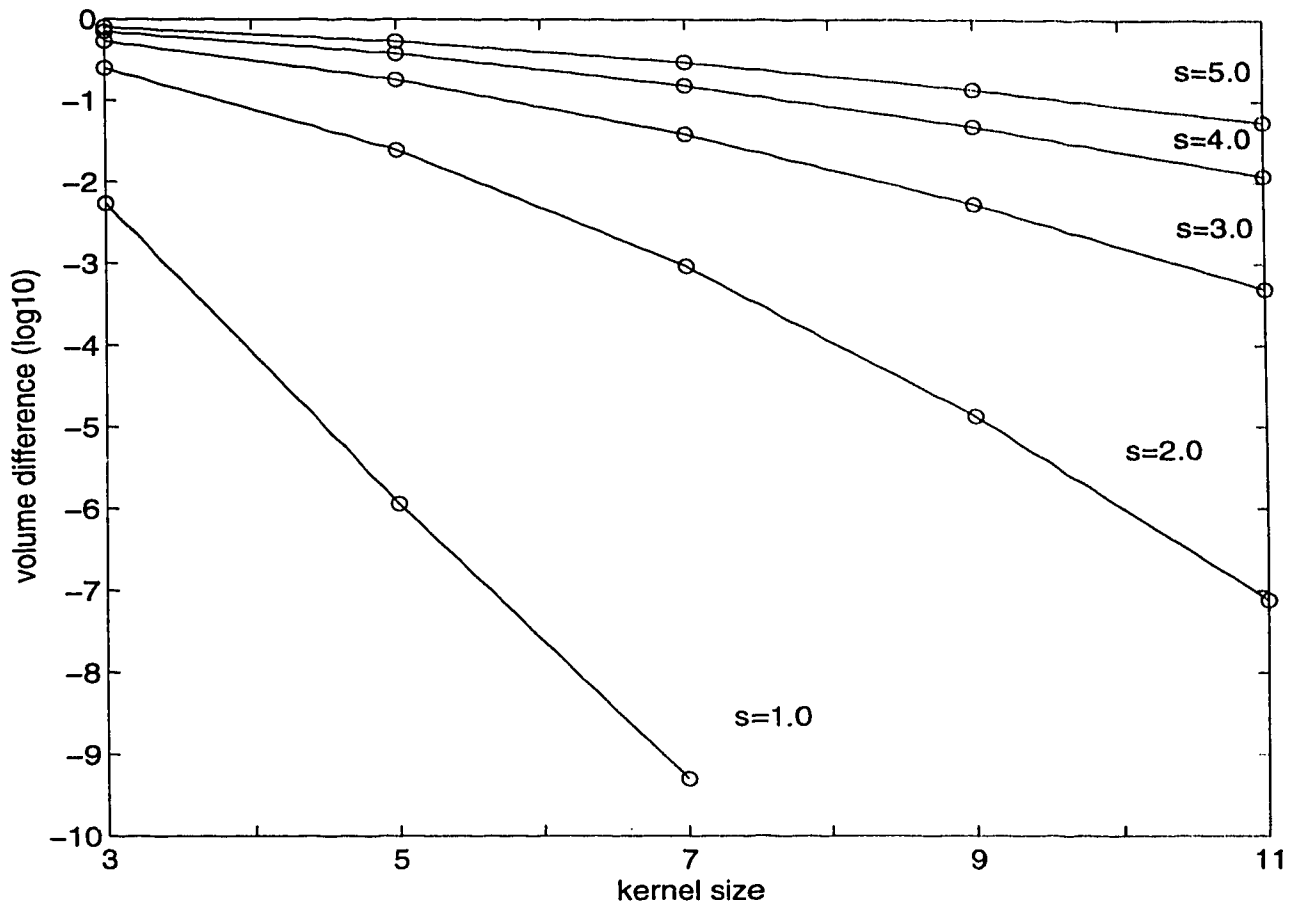


Figure 3.5: Volume difference by kernel size (nxn) and Gaussian width (sigma) as compared with the theoretical volume of 1.0

equation for a block sampling a two-dimensional function is given in equation 3.37.

$$\bar{g}(i, j) = \int_{i-1/2}^{i+1/2} \int_{j-1/2}^{j+1/2} g(x, y) dx dy \quad (3.37)$$

A visual comparison between the two techniques for discrete sampling is shown using the two-dimensional Gaussian in figure 3.6. The effects of  $\sigma$  on the volume of a discretely sampled Gaussian kernel is shown in table 3.1. As can be seen in the table, the direct sampling method results in a kernel whose volume is not unity for small values of  $\sigma$ . The size of the kernel has been chosen to be much larger than would be practically used. Even with the large kernel size there is still a small percentage of the volume that lies outside the kernel and therefore the volumes do not remain at 1.0 for large values of  $\sigma$ . Since it is desirable to maintain a constant Gaussian kernel volume regardless of the choice of  $\sigma$ , the block averaged method was used to sample the Gaussian and its derivatives as needed.

	$\sigma$							
	0.50	0.75	1.0	1.5	2.0	3.0	4.0	5.0
$\sum \sum g(i, j)$	1.02897	1.00006	1.00000	1.00000	1.00000	.999943	.996544	.975603
$\sum \sum \bar{g}(i, j)$	1.00000	1.00000	1.00000	1.00000	1.00000	.999938	.996447	.975316
$\sum \sum  g(i, j) - \bar{g}(i, j) $	.312135	.096505	.057719	.026352	.015211	.006770	.003830	.002446

Table 3.1: Sampled vs. Block averaged discrete Gaussian kernels

## Derivatives

Using the relationship given in equation 3.37 the resulting block averaged Gaussian and derivative functions are:

$$\frac{\partial \bar{g}(i, j)}{\partial i} = \frac{\left( e^{-\frac{(2i+1)^2}{8s^2}} - e^{-\frac{(2i-1)^2}{8s^2}} \right) \left( \operatorname{erf}\left(\frac{\sqrt{2}(2j+1)}{4s}\right) - \operatorname{erf}\left(\frac{\sqrt{2}(2j-1)}{4s}\right) \right)}{2\sqrt{2\pi}s^{-1}} \quad (3.38)$$



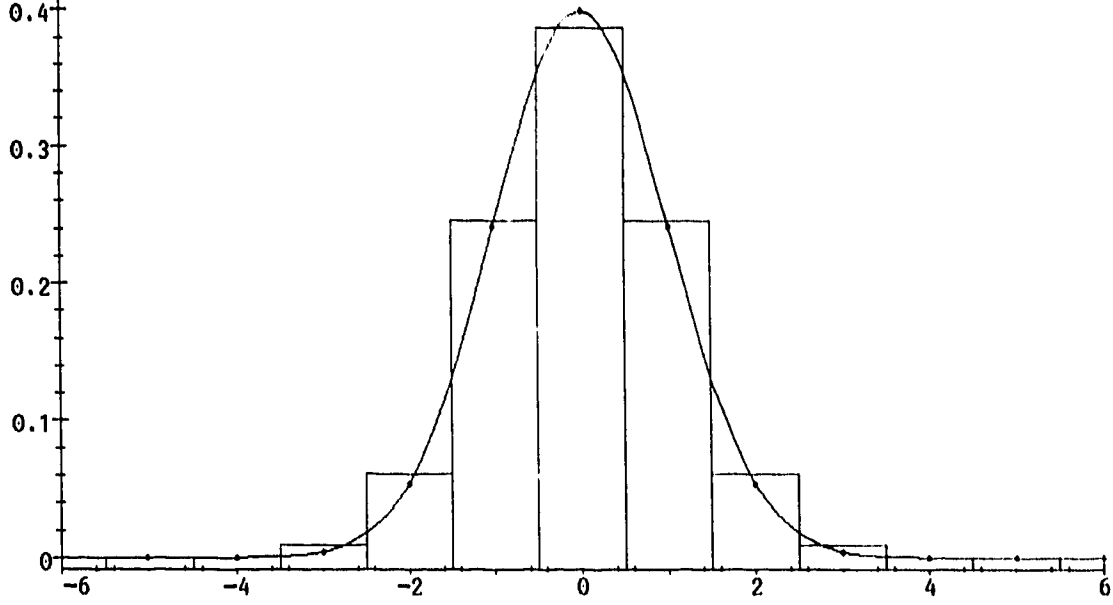


Figure 3.6: A one-dimensional Gaussian with  $\sigma = 1.0$

$$\frac{\partial \bar{g}(i, j)}{\partial j} = \frac{\left( \operatorname{erf}\left(\frac{\sqrt{2}(2i+1)}{4\sigma}\right) - \operatorname{erf}\left(\frac{\sqrt{2}(2i-1)}{4\sigma}\right) \right) \left( e^{-\frac{(2j+1)^2}{8\sigma^2}} - e^{-\frac{(2j-1)^2}{8\sigma^2}} \right)}{2\sqrt{2\pi}\sigma^{-1}} \quad (3.39)$$

$$\frac{\partial^2 \bar{g}(i, j)}{\partial i \partial j} = \frac{\left( e^{-\frac{(i+1/2)^2}{2\sigma^2}} - e^{-\frac{(i-1/2)^2}{2\sigma^2}} \right) \left( e^{-\frac{(j+1/2)^2}{2\sigma^2}} - e^{-\frac{(j-1/2)^2}{2\sigma^2}} \right)}{2\pi\sigma^2} \quad (3.40)$$

$$\frac{\partial^2 \bar{g}(i, j)}{\partial i^2} = \frac{\left( e^{-\frac{(i+1/2)^2}{2\sigma^2}}(2i+1) - e^{-\frac{(i-1/2)^2}{2\sigma^2}}(2i-1) \right) \left( \operatorname{erf}\left(-\frac{(j+1/2)}{\sqrt{2}\sigma}\right) - \operatorname{erf}\left(-\frac{(j-1/2)}{\sqrt{2}\sigma}\right) \right)}{2\pi\sigma^2} \quad (3.41)$$

$$\frac{\partial^2 \bar{g}(i, j)}{\partial j^2} = \frac{\left( e^{-\frac{(j+1/2)^2}{2\sigma^2}}(2j+1) - e^{-\frac{(j-1/2)^2}{2\sigma^2}}(2j-1) \right) \left( \operatorname{erf}\left(-\frac{(i+1/2)}{\sqrt{2}\sigma}\right) - \operatorname{erf}\left(-\frac{(i-1/2)}{\sqrt{2}\sigma}\right) \right)}{2\pi\sigma^2} \quad (3.42)$$

Where the error function  $\operatorname{erf}$  is defined as:

$$\operatorname{erf}(x) = \int_0^x \frac{2}{\pi} e^{-t^2} dt \quad (3.43)$$

Kernels were created using values from these functions as one of the necessary steps for approximating the curvature of the scoliotic back surface.

Implementing the direct interpretation of equation 3.29 does not quite yield the desired derivative result when using the Gaussian. Weiss's work on high-order differentiation filters [42] suggested that the Gaussian was not suitable for finding derivatives greater than the first order. Contrary to this information, Blom [24] concluded that determining derivatives, even for high orders, combined with scale space (the Gaussian operator), was a very robust and stable operation. Since the determination of second order derivatives is necessary for the calculation of curvature it was necessary to determine if the Gaussian was capable of providing stable second order derivatives for use in the convolution operation. Since the choice of  $\sigma$  could be selected out a range of values, it is necessary for the derivatives to provide consistent results regardless of the  $\sigma$  value. To test the stability of the Gaussian derivative kernels the first derivative of an arbitrarily chosen third degree polynomial ( $x^3 + 5x^2 + 12$ ) was compared with the Gaussian convolution approach as shown in figure 3.7. The arbitrary decision concerns the coefficients of the polynomial and not the degree of the polynomial. The degree of the polynomial was chosen to best reflect a contour that could be produced by examining a cross-section of the back surface in a region where the surface has large height variations. A first degree polynomial would imply that a cross-section of the back surface could be represented by a straight line which is very unlikely. A second degree polynomial could possibly be used to represent some back surfaces where the changes in elevation are very subtle. Polynomials of degree higher

than three could become susceptible to small variations in surface elevation due to noise and consequently produce inaccurate representations. The Gaussian used in the convolution was generated with  $\sigma$  values of 0.8, 0.9, 1.0 and 1.1. The minimal range of  $\sigma$  was used only for a better comparison with the range used in the second derivative case which had to be limited. All values of  $\sigma$  used overlap the curve in the figure 3.7 demonstrating that the first derivative of the Gaussian kernel is not susceptible to variations in  $\sigma$ .

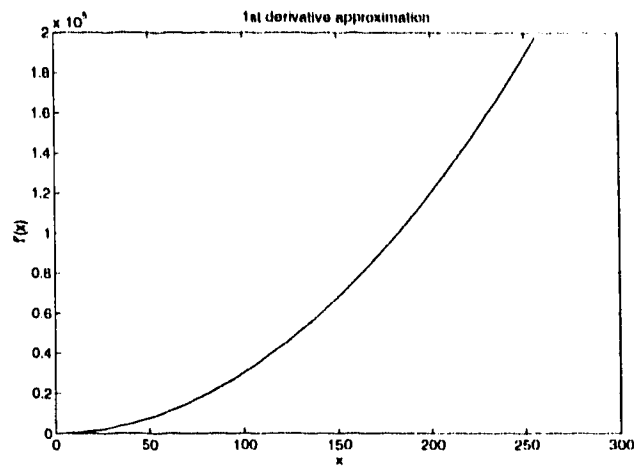


Figure 3.7: First derivative of  $x^3 + 5x^2 + 12(3x^2 + 10x)$  compared with Gaussian approximations

An example is provided in figure 3.8 which demonstrates the instability of the Gaussian's second derivative to approximate the second partial derivative of a third degree polynomial function when used in the convolution operation. The  $\sigma$  values used are 0.8,0.9,1.0, and 1.1. Large values of  $\sigma$  would not be visible on the provided scale of the graph. The exact value of the derivative is the straight line equation  $y = 6x + 10$ .

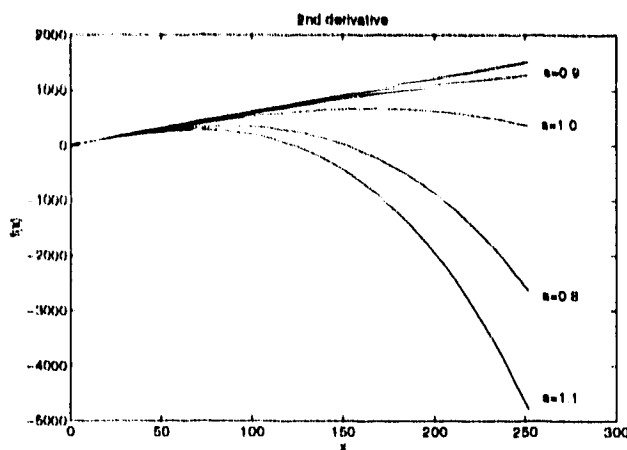


Figure 3.8: Second derivative of  $x^3 + 5x^2 + 12$  compared with Gaussian approximations

Now although the experimental results demonstrate that using the second derivative of the Gaussian is not stable, the Gaussian may still be used. These results suggest that a kernel that contains values directly sampled from the second partial derivative of a Gaussian should not be used. This concurs with Weiss' statement about the Gaussian only being stable for direct determination of first order derivatives. Although Blom provides a strong mathematical justification for his stand on the stability of the Gaussian for higher order derivatives, (he provides experimental results up to the fourth derivative) it is unclear from his paper [24] how the various partial derivative Gaussian kernels were implemented. Weiss [42] describes how to design a better filter that can be tuned to provide the necessary derivatives up to a given order. Weiss' power-preserving filters will not be examined further but a part of his filter creation method will be used. Since the second partial derivative of the Gaussian is absolutely necessary for curvature calculation and because the instability of the Gaussian prevents the direct use of a second partial derivative, another method

must be used to provide the necessary convolution kernels. This other method was used by Weiss and is another property of the convolution operator. The property that will be used is:

$$D^n = D * D \dots \quad (3.44)$$

where  $D^n$  is the  $n$ th order derivative operator. The concept intuitively makes sense. If a first order partial derivative kernel is convolved with an image the result will be a scaled version of the first order partial derivative of the image. If that resultant image is again convolved with the same kernel, the result will be the second partial derivative of the image - exactly what we are looking for! Equation 3.44 doesn't exactly express this relationship, however. It can be interpreted as stating that to get the  $n$ th order partial derivative kernel, convolve a first order partial derivative  $n - 1$  times. Convolve this resultant kernel with an image would provide the  $n$ th order partial derivative data. Using this method, the second order partial derivative of the example polynomial used previously ( $x^3 + 5x^2 + 12$ ) was determined for multiple values of  $\sigma$ . A plot of the resultant curves is shown in figure 3.9. As can clearly be seen, all of the determined derivative curves are exactly the same -  $y = 6x + 10$ . This procedure is used to calculate the necessary second order partial derivatives of the back surface data. The cost for performing two convolutions on the data is that there is an even larger loss of data points at the borders attributed to compensation for the edge effect of discrete convolution described earlier. There will be a loss of  $N - 1$  data points at each edge of the back surface array. This can be seen clearly by the black borders surrounding the shape analysis images shown in the results section to

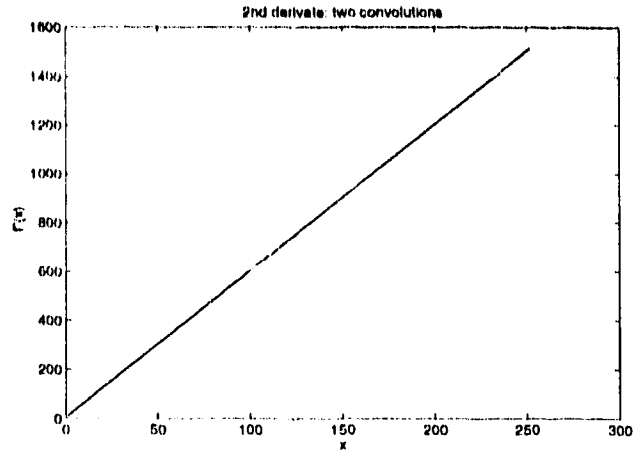


Figure 3.9: Second derivative approximation using two convolutions

follow (chapter 6).

# Chapter 4

## Shape Representation

The need for invariance and scale independence lead to the selection of shape as the surface property by which scoliotic back surfaces would be analyzed. Trying to describe the shape of a complex surface such as a scoliotic back is not a simple task. In order to analyze such a surface it is necessary to reduce the complexity. Simplifying the surface to be analyzed will be done by partitioning the surface into a few regions that share a similar attribute. The attribute itself can vary depending on how the calculated curvature values are used. As will be shown, surfaces can be partitioned into as many regions as one would like depending on how the curvature values are used.

### 4.1 Defining shape

The human visual system is very adept at distinguishing the shape of objects. We are able to discern if two items although possibly differing in size, orientation, texture or color have the same shape. In the previous chapters techniques have been

described on how to obtain curvature information given a surface defined as a height field above a reference plane - a Monge patch. The range of values for the computed curvatures are theoretically limitless but practically limited by the precision of the hardware on which the program is being executed. In this thesis the practical limits for computed curvature are based on the precision of a *double precision floating point* value as implemented by the Hewlett Packard PA-RISC machines - [4.94066e-324,1.79769e+308]. The discrete sampling of the patient's back images to produce the Monge patch limits the accuracy of the data by which the curvature is calculated. Consequently, for the same back surface the curvature determined for the same location in separately acquired images may have different values. Since there will be some error associated with every calculated curvature value the range of curvature will become segmented into an indeterminate number of regions defined by  $\kappa \pm \epsilon$ . Many researchers [2][40][12][25] have found it useful to classify the curvature of a surface into a small number of regions. Goldgof [12] used thresholding of absolute Gaussian curvature to determine "feature" points for matching terrain. Frobin [40] used the sign of the Gaussian curvature to define elliptic ( $K > 0$ ), parabolic ( $K = 0$ ) and hyperbolic ( $K < 0$ ) regions. Koenderink [26] derived a shape index to categorize shape into nine regions. Other possible segmentation schemes noted by Arman [2] are 1) using curvatures  $\kappa_1$  and  $\kappa_2$  to distinguish four distinct regions and 2) using both the Gaussian (K) and mean (H) curvature values to provide more information to define six distinct regions. Examples of some of the various classifications of shape applied to scoliotic back surface data are shown in figure 4.1. The original back surface data



consists of an array of depth values which are mapped to a grayscale or color scheme.

The closer points are brighter while the more distance points are darker.

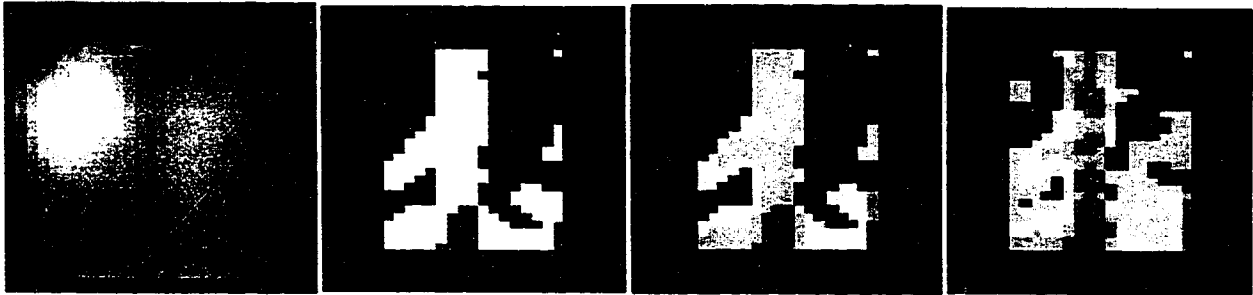


Figure 4.1: From left to right: depth map,  $K$  sign map,  $H$  and  $K$ , shape index Examples of surface partitioning by different shape classifications.

## 4.2 Principal Curvatures

In his survey of classification techniques Arman [2] describes a shape classification based on principal curvature signs (Table 4.1). This is what Frobin [15] used in his

	$\kappa_1 > 0$	$\kappa_1 = 0$	$\kappa_1 < 0$
$\kappa_2 < 0$	saddle	ridge	peak
$\kappa_2 = 0$	valley	flat	ridge
$\kappa_2 > 0$	pit	valley	saddle

Table 4.1: Classifying Surface Types Using Principal Curvature Information

first examination of back surface shapes and was also used by Besl [10]. Frobin also used the magnitude and direction of the principal curvatures as another visual representation in the qualitative analysis of scoliotic back deformity. Frobin [40] provides an example of a back surface representation using principal curvature information which is shown in figure 4.2. In the image the length of the axes are proportional

to the magnitude of the principal curvatures. The orientation of the lines is based on the angle of the principal curvatures. The magnitude of the principal curvatures determined in equation 3.18 are:

$$\kappa_{1,2} = \frac{EN + GL - 2FM \pm \sqrt{(EN + GL - 2FM)^2 - 4(EG - F^2)(LN - M^2)}}{2(EG - F^2)} \quad (4.1)$$

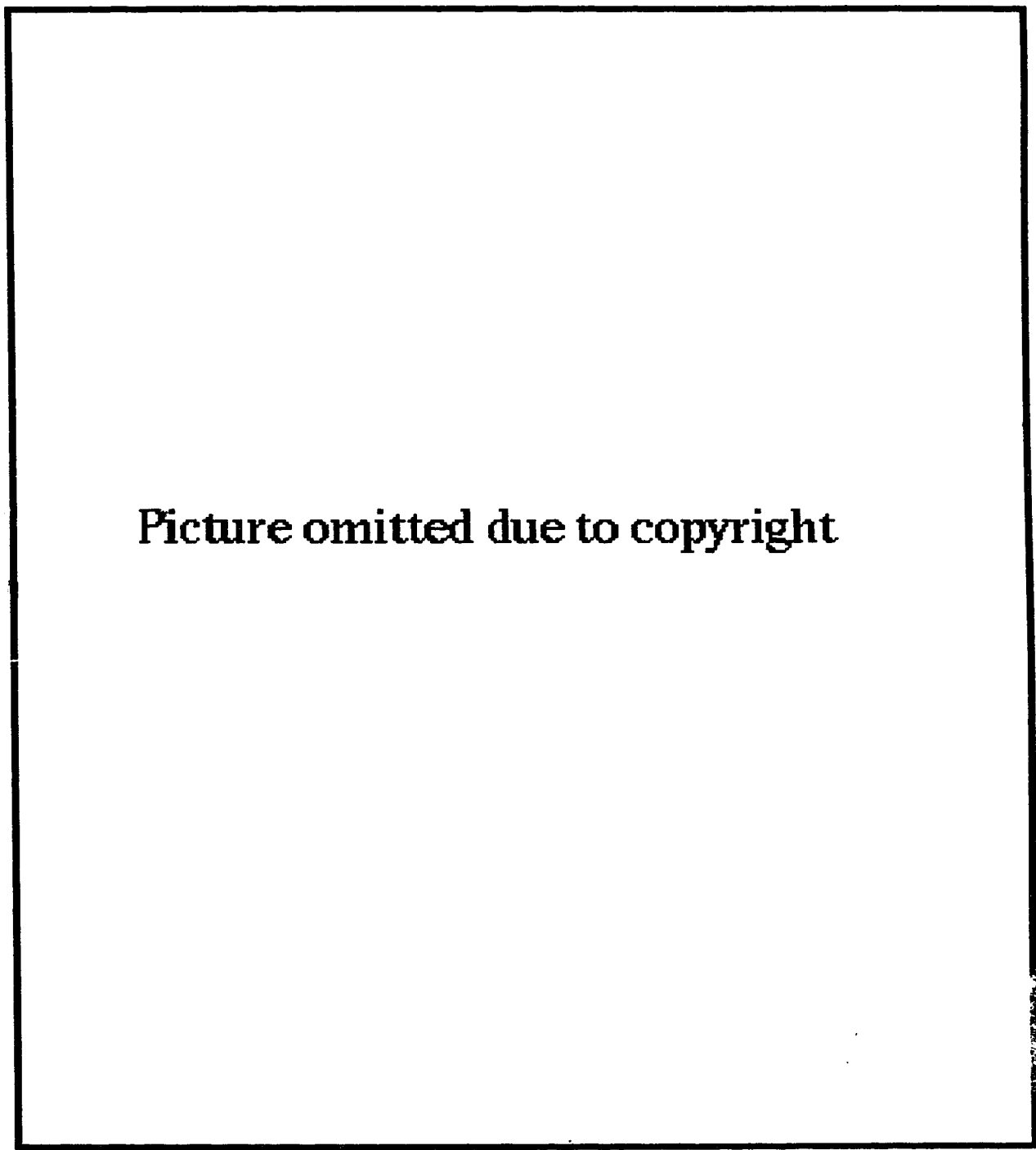
where the larger value is referred to as the maximum curvature  $\kappa_1$  and the lesser value is referred to as the minimum curvature  $\kappa_2$ . The direction of the principle curvatures on the surface is given by equation equation 3.19. In particular the maximum and minimum principal directions are:

$$\phi_{1,2} = \tan^{-1} \left( \frac{-B \pm \sqrt{B^2 - AC}}{C} \right) \quad (4.2)$$

where  $A = EM - FL$ ,  $2B = EN - GL$ ,  $C = FN - GM$

### 4.3 Gaussian and mean curvature

Gaussian and mean curvature have been the most commonly used measures of curvature. Frobin, Hierholzer and Drerup have been very innovative in application of mathematical techniques to scoliotic research. In particular, [40] and [15] describe the use of scoliotic back curvature to help evaluate the progress of deformity while [17] and [13] describe the use of curvature to find anatomical “landmarks” on the back surface. Although the work by Frobin was only used for qualitative analysis of the back surface, it did provide inspiration to attempt to use similar means for quantitative analysis.



**Picture omitted due to copyright**

Figure 4.2: Principal curvatures and directions of a scoliotic back surface

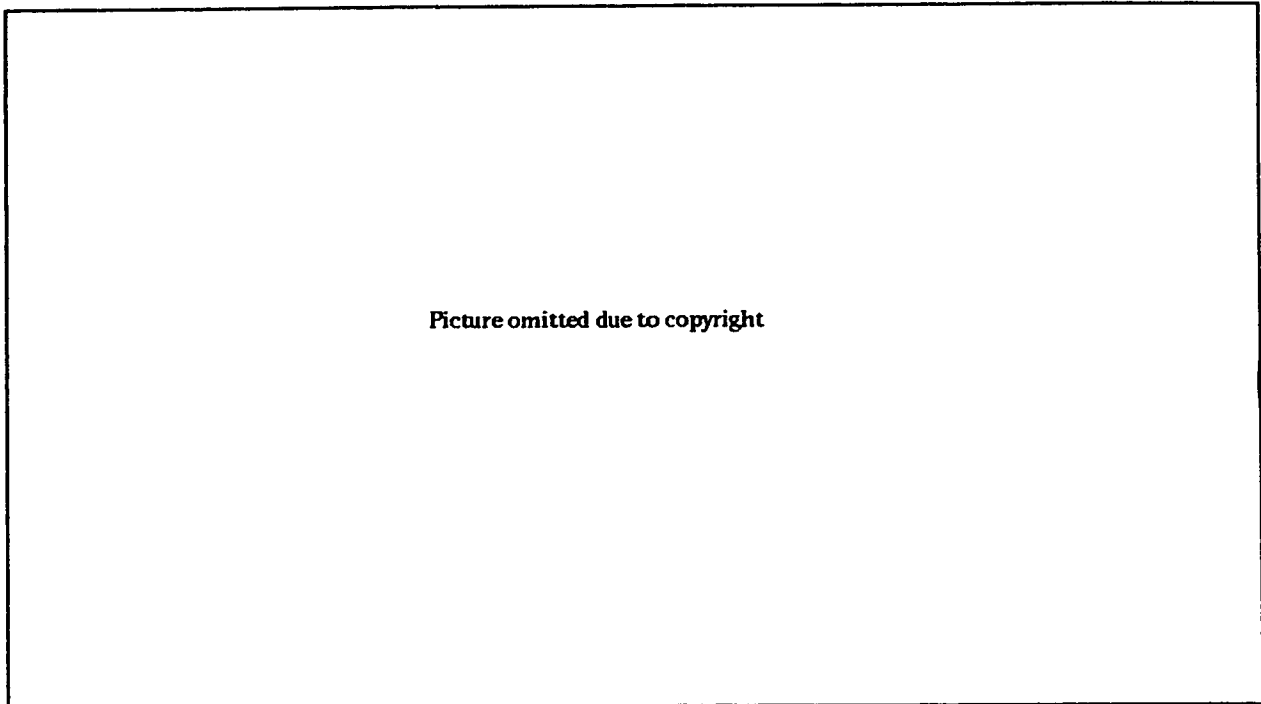


Figure 4.3: Gaussian (left) and mean (right) curvature

The range of possible curvature values is from negative infinity to positive infinity. There are two choices for dividing this range of values in an attempt to reduce the number of curvature classifications: by sign or by magnitude. Separation by sign is a simple solution but the regions it produces are very coarse and may not be informative. In his analysis of human back shape, Frobin [40] first scaled the calculated values of curvature logarithmically, and then experimentally found adequate partitioning points. Figure 4.3 shows an example of Frobin's partitioning of a scoliotic back using Gaussian and mean curvature. Besides using the Gaussian and mean curvatures separately, Arman [2] notes that a combination of the two curvatures can produce an eight region shape classification. This classification is shown in table 4.2.

	$\kappa > 0$	$\kappa = 0$	$\kappa < 0$
$H < 0$	peak	ridge	saddle ridge
$H = 0$	-	flat	minimal
$H > 0$	pit	valley	saddle valley

Table 4.2: Classifying Surface Types Using Gaussian and Mean Curvature Information

#### 4.4 Shape Index

Koenderink and van Doorn [26] define a shape index which encompasses the intuitive properties of shape. Koenderink states that although Gaussian and mean curvature are informative they do not by themselves capture the intuitive notion of “local shape” - thus both are necessary. The best option is described as using a combination of the principal curvatures. The shape index is derived from an analysis of the curvature parameter plane shown in figure 4.4. Using a polar coordinate system, the length of a half-ray from the origin represents size and the angle of the half-ray denotes the

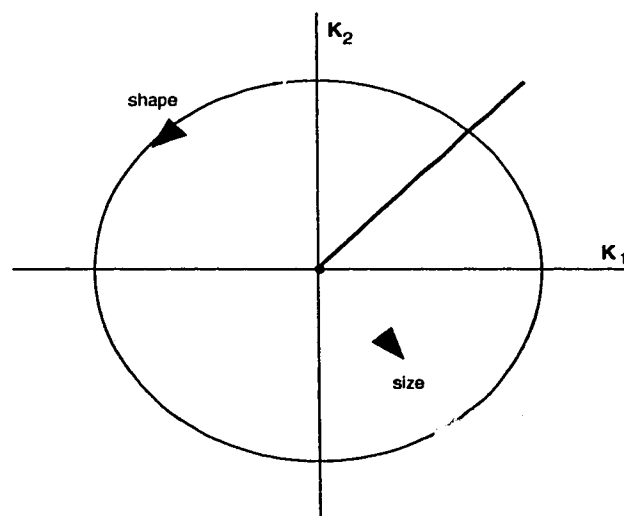


Figure 4.4: Curvature parameter plane

local shape at the point being examined on the surface. The noteworthy properties of the polar representation are:

- the origin represents the uncurved patch
- all points of a half-ray from the origin represent the same shape, although the shapes differ in size
- diametrically opposite points at an equal distance from the origin represent surfaces that fit together - *complementary* shapes
- points at an equal distance from the origin, related through a reflection at the axis  $\kappa_1 = \kappa_2$ , are congruent
- points on the line  $\kappa_1 = -\kappa_2$  at an equal distance from the origin are simultaneously complementary and congruent

The problems that arise from this approach to defining the space of shapes are two-fold:

- using the (two-sided) rays of the  $(\kappa_1, \kappa_2)$ -plane, you cannot distinguish between inside and outside
- using half-rays leads to the same shape appearing twice in shape space

Koenderink and van Doorn picture the space of shapes as having the topology of a 1-dimensional disc as shown in figure 4.5. This is clearly brought out through their

definition of a *shape index* as given in equation 4.3. The use of the arctangent function limits the range of shape indices from -1 to +1. As with the normal convention,  $\kappa_1$  refers to the maximum curvature value.

$$(\text{Shape index}) s = \frac{2}{\pi} \tan^{-1} \left( \frac{\kappa_2 + \kappa_1}{\kappa_2 - \kappa_1} \right), \kappa_1 \geq \kappa_2 \quad (4.3)$$

All patches, except for the planar patch which has an indeterminate shape index as should be, map on the segment  $s \in [-1, +1]$ . This representation highlights the “natural” properties that are intuitive of shape. These properties include:

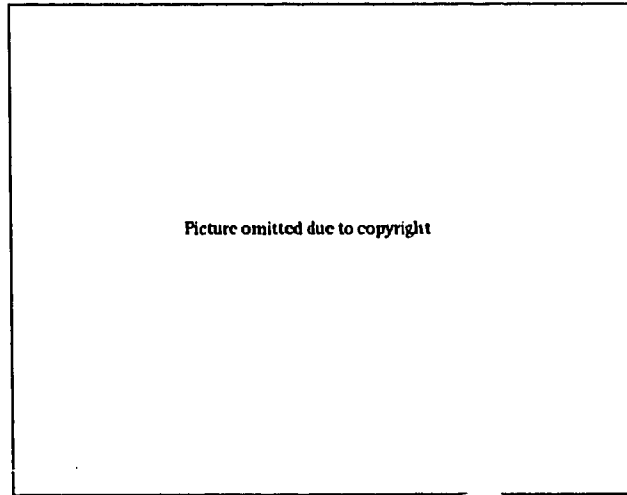


Figure 4.5: Koenderink’s shape space plane

- two shapes for which the shape index differs merely by sign represent complementary pairs
- the shape for which the shape index vanishes, and consequently has indeterminate sign, represents the objects which are congruent to their own moulds
- convexities and concavities find their places on opposite sides of the shape scale

- the shape index scale is uniformly covered since it is directly proportional to the angle with the  $\kappa_1 + \kappa_2 = 0$  axis
- the endpoints represent the outside ( $s = 1$ ) or the inside ( $s = -1$ ) of a spherical surface

The segmentation of the shape index scale is given in table 4.3 with pictures of the various shape types shown in figure 4.6. The shape types range from the purely concave when  $s = 1$  to the purely convex when  $s = -1$ . The intermediate shape types are formed by changing the principal axes from one extreme to the other. When surfaces are segmented by shape classifications methods, colour may be used to visually distinguish the different shape types. Colours are usually selected to maximize contrast and are based on user preference. However, the choice of colours for the different shape index ranges is not arbitrary. Koenderink and van Doorn [26] devised a colour scheme that had the following properties:

- convexities, concavities and saddle shapes should perceptually segregate. They should be assigned hues that are highly distinguishable.
- recognizable hues should be used: red, green, blue, yellow and white
- extremes should be clearly visible
- complementary shapes should be represented by complementary hues
- the shape index scale should map on a continuous curve in colour space



<i>Mnemonic</i>	<i>Index range</i>	<i>Colour name</i>	<i>(R, G, B)</i>
Spherical cup	$s \in [-1, -7/8)$	Green	(0,1,0)
Trough	$s \in [-7/8, -5/8)$	Cyan	(0,1,1/2)
Rut	$s \in [-5/8, -3/8)$	Blue	(0,1,1)
Saddle rut	$s \in [-3/8, -1/8)$	Pale Blue	(1/2,1,1)
Saddle	$s \in [-1/8, +1/8)$	White	(1,1,1)
Saddle ridge	$s \in [+1/8, +3/8)$	Pale Yellow	(1,1,1/2)
Ridge	$s \in [+3/8, +5/8)$	Yellow	(1,1,0)
Dome	$s \in [+5/8, +7/8)$	Orange	(1,1/2,0)
Spherical cap	$s \in [+7/8, +1]$	Red	(1,0,0)

Table 4.3: Classifying Surface Types Using Shape Index

The work in this thesis will present visual representations of surface shapes to the user. The colour scheme suggested by Koenderink [26] was used since it helps to distinguish the shape regions in a simple manner.

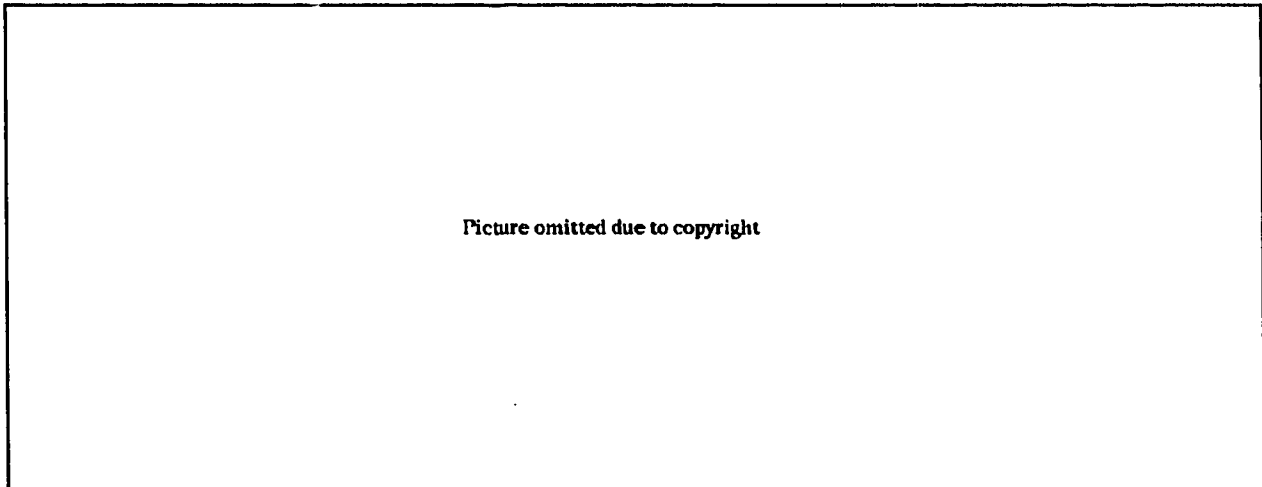


Figure 4.6: Shape classifications according to shape index scale

## 4.5 Other classifications

### 4.5.1 Ridge and Groove

In addition to the use of principal curvatures, Gaussian curvature, and mean curvature, Frobin [40] employed a shape classification which he described as “ridge and groove” curvature. The benefit of the “ridge and groove” curvature was that it emphasized the regions where there was a large difference between the principal curvatures. Frobin admits to choosing the shape classifications arbitrarily but the selections provided an objective means by which asymmetry of the back could be detected. Frobin’s definition of “ridge and groove” curvature is given in equation 4.4.

$$R = (\kappa_1 - \kappa_2 * \text{signum}^1(\kappa_1 * \kappa_2))/2 \quad (4.4)$$

### 4.5.2 Gaussian feature points

Another method of using curvature magnitude to segment the curvature range into fewer regions is to use extreme values. Goldgof [12] uses Gaussian curvature to aid in extracting features for use with terrain matching. Unlike Besl and Jain [10] who used both Gaussian and mean curvature analysis in their work, Goldgof uses only large values of Gaussian curvature. The advantage of this approach is that the feature matching is less susceptible to noise. To limit the number of extreme points for matching, Goldgof had to select a threshold level. The choice of this threshold affected

---

<sup>1</sup>signum( $x$ ) returns either -1, 0 or 1 depending on the sign of  $x$  being less than 0, equal to 0, or greater than 0 respectively.

the number of points that were produced and available for matching and was selected based on experimental results and is application dependent.

#### **4.6 Summary**

There are many ways to represent the shape of a surface. The primary methods involve the Gaussian and mean curvatures either directly or in some combination. This work will only examine those classifications techniques that can subdivide the surface into a fixed set of shape regions. These classifications include the Gaussian and mean curvature combination, shape index, and the sign of the principal curvatures. Since the back surface data that will be analyzed is of a discrete nature, it will be necessary to implement discrete algorithms to calculate the surface curvatures.

# Chapter 5

## Applying shape analysis

A large surface such as a scoliotic back is too complex to be described as a whole. Partitioning the surface into small, similarly characterized regions was previously discussed as a means of reducing the difficulty for a quantitative description of the back surface. Quantitative analysis can then be performed by determining useful parameters for each of these shape regions.

### 5.1 Obtaining information from shape regions

It would be difficult to observe changes on a patient's scoliotic back if all that could be monitored were hundreds of individual points with some curvature value. For this reason the back surface was segmented to reduce the features of interest to a few regions of similar shape. From these regions we wish to quantify the change of shape in a scoliotic back over a period of time as measured by two digitized back surface data sets. Since there is no apriori knowledge as to what type of measure will best provide this information I can but offer a few formula that may meet this goal.

The quantities calculated for each of the shape regions are: estimated surface area, projected surface area, and the magnitude and direction of the principal curvatures.

### 5.1.1 Estimated surface area

In his paper discussing intrinsic and extrinsic surface characteristics, Besl [8] described an intrinsic quantity which is the determinant of the first fundamental form matrix:

$$s_{area} \approx \sqrt{E(G - F^2)} \quad (5.1)$$

This quantity, when summed over a region, can provide an estimate of the surface area of that region.

### 5.1.2 Projected surface area

Projected surface area is merely a count of the number of samples within a region. It is provided as a reference value since it directly characterizes size.

### 5.1.3 Principal Curvatures

The resultant magnitude and angles of the principal directions for a region are determined by taking the average of the values at each point in the region.

## 5.2 Accounting for size

These measurements by themselves do not account for the scale of the object however. As mentioned earlier, shape was chosen as a suitable surface characteristic to measure

because of its independence from size. Many of the mentioned quantities from which measurements are made are very dependent on the number of data points composing a surface. To remove this dependence, a scale factor should be applied which would normalize the results. If all that was required was to make the surfaces the same size this could be trivially solved by scaling the image and interpolating data as required. Because we are dealing with data that may be used for diagnostic purposes, this type of solution is not acceptable. Rescaling the back surface data in such a manner would distort the back surface features making any interpretation of the analysis suspect. A possible solution to this problem is to use the curvedness measurement described by Koenderink and van Doorn [26]. While investigating a measurement of shape, Koenderink found it useful to provide a measure of the intensity of the surface curvature. Whereas his shape index provides a measure of shape, his *curvedness* provides a measure of size. Relating back to Koenderink’s one-dimensional disc or “linear segment” analogy of shape space, the scale index relates to the angle along the segment and the *curvedness* relates to the distance from the origin. This provides the mathematical definition for *curvedness* as:

$$c = \sqrt{\frac{\kappa_1^2 + \kappa_2^2}{2}} \quad (5.2)$$

Unlike the unitless shape index, curvedness has the units of reciprocal length. Thus, in order to “normalize” an area measurement the value would have to be multiplied by the square of the curvedness value.

### 5.3 Determining equality

Regions are divided up into separate planes according to values for the particular shape classification technique being used. Given a point from one image the appropriate plane is selected by examining the shape classification value of the point. Each region in the corresponding plane is searched to see if the point is within its bounding box. Once found, the parameters for that regions are retrieved. The same plane is retrieved in the opposing image and each of the regions there are compared with the parameters from the selected region in the first image. The region that best matches all the parameters is determined to be the corresponding region.

# Chapter 6

## Experimental results

### 6.1 Which kernel to use?

As discussed earlier, two kernels could be used to provide approximations for the partial derivatives necessary for calculating surface curvatures. The same third degree polynomial used for demonstrating the deficiency of the Gaussian kernel implementation,  $x^3 + 5x + 12$ , was also tested with the directional derivative kernel. The kernels used for approximating the first and second partial derivatives were:

$$\vec{r}_u = \begin{bmatrix} 1 & 0 & -1 \end{bmatrix} \quad \text{and} \quad \vec{r}_{uu} = \begin{bmatrix} 1 & -2 & 1 \end{bmatrix}$$

The resulting convolutions were compared against the actual data corresponding to the appropriate derivative and are shown in figures 6.1 and 6.2. Figures 3.7 and 3.9 demonstrated that the Gaussian convolution method could reliably produce derivatives for a third degree polynomial. The directional derivative was shown to produce



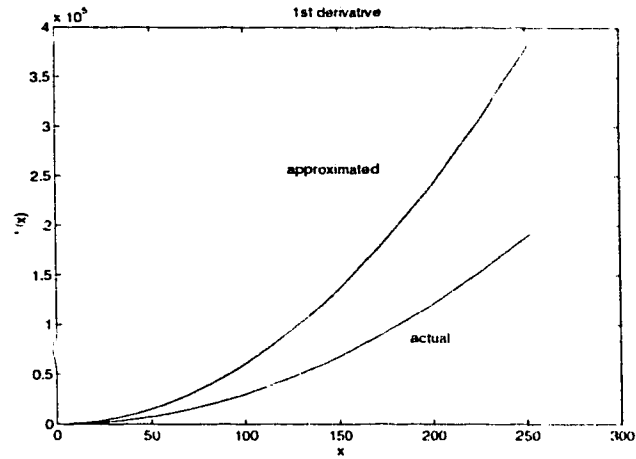


Figure 6.1: First derivative of  $x^3 + 5x^2 + 12$  compared with directional derivative approximation.

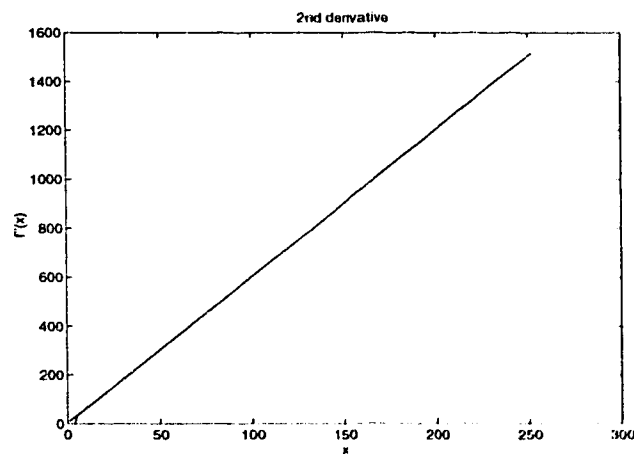


Figure 6.2: Second derivative of  $x^3 + 5x^2 + 12$  compared with directional derivative approximation. (Actual and determined results overlap)

a poor approximation for the first partial derivative of the same polynomial but did provide a good approximation of the second partial derivative. Scoliotic back surfaces can vary in the degree of deformity which can be compared to the degree of a polynomial that could be used to approximate the surface where it intersects a transverse plane. For back surfaces that exhibit little deformity, the polynomial may be of a lower degree and thus both the directional derivative and the Gaussian derivative would provide a reasonable approximation of the actual surface derivatives. However, if the back surface exhibited a prominence of one scapula for instance, the variation in the surface would need a polynomial of a higher degree to represent it. In such a case, the first order derivative approximations provided by the directional derivative kernel could be inaccurate. Of course, this relationship of polynomial order to back surface deformity is only speculative.

## 6.2 Visual assessment of shape classifications

A visual comparison was performed to see if the shape classification regions looked similar using both kernel methods. The shape classifications are provided in the legend shown in figure 6.3. The colour scheme proposed by Koenderink and van Doorn [26] is used for all the classification methods - not just the shape index method. In cases where the number of possible classifications is not the same, the most similar shape was used to provide the colour value. For instance, flat regions described in the Gaussian and mean curvature classification would be matched with the saddle region of the shape index classification since both represent shapes near the middle of their

respective shapes range<sup>-</sup>. Since the Gaussian convolution method inherently smooths the data, a normalized Gaussian kernel of the same size was used to provide the same filtering effect on the back data before Frobin's kernels (section 3.4.1) were applied. Images produced using Frobin's kernels on back surface data smoothed beforehand with a 3 x 3 Gaussian kernel are shown in figure 6.4. For all tests the Gaussian width ( $\sigma$ ) was set to 1.0. Images produced using Gaussian derivative kernels of size 3 x 3 are shown for comparison in figure 6.5.

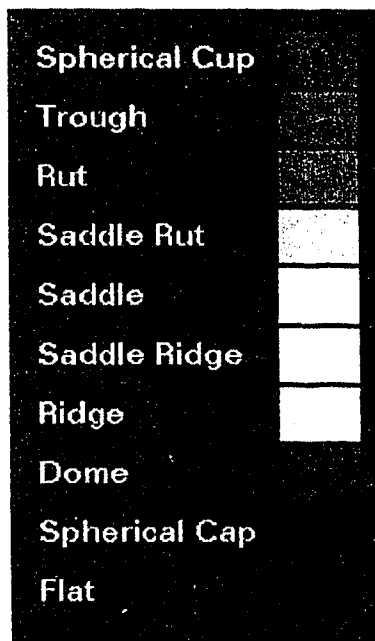


Figure 6.3: Shape classification colour legend



Figure 6.5: From left to right: K sign map, H and K, shape index  
Shape classifications using a Gaussian kernel (3x3)

The two methods appear to be quite similar with the exception of the shape index classified image. Frobin's kernels do not appear to be able to adequately supply enough accuracy for the shape index classification to be able to distinguish more than a few regions. The Gaussian convolution method allows the production of all the shape classification regions even though the kernel size is small (3x3).

Using a larger kernel size, the same tests were repeated. Images produced using Frobin's kernels on back surface data smoothed beforehand with a  $7 \times 7$  Gaussian kernel are shown in figure 6.6. The images produced using Gaussian derivative kernels

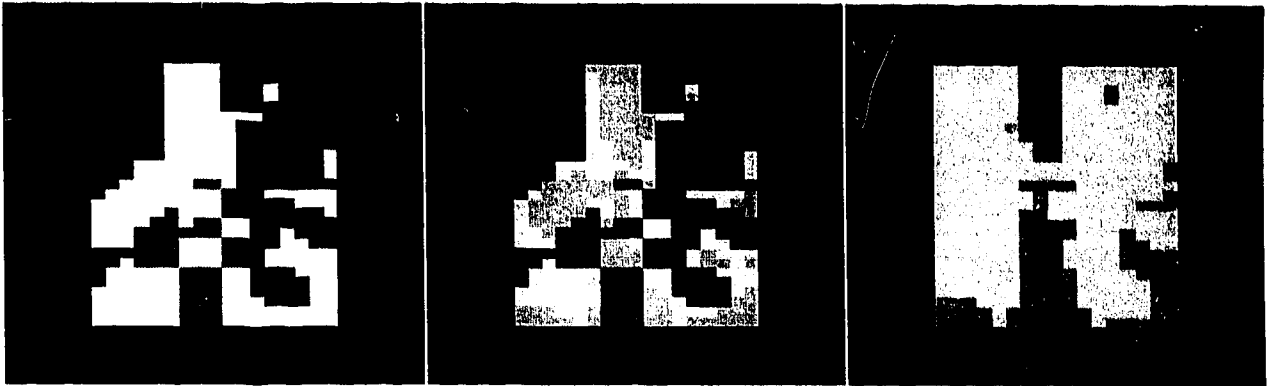


Figure 6.6: From left to right: K sign map, H and K, shape index

of size  $7 \times 7$  are shown below in figure 6.7. Again the two methods appeared to produce

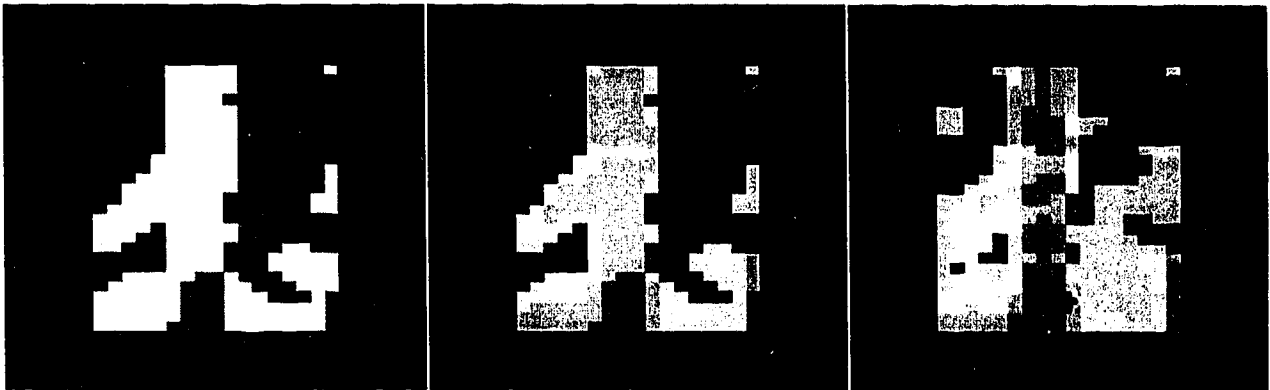


Figure 6.7: From left to right: K sign map, H and K, shape index

similar results except for the shape index classification. The Gaussian convolution method also seemed to produce regions that were in general more homogeneous. The homogeneity of a shape classified region is important since the connectivity algorithm used to identify regions requires that there be no separation between similarly valued points.

### 6.3 Testing

Testing of the techniques suggested to quantize the shape of scoliotic backs was needed to ensure that the requirements of invariance to orientation and scaling had been met. The measured parameters for the shape regions were tested for accuracy as the test surface  $v$  rotated and scaled. In addition tests were conducted to determine the dependence on  $\sigma$  since a Gaussian was used in the determination of curvature values. The tests conducted in this work have primarily used synthesized data. There are a number of reasons as to why this was done.

- the need to establish the validity of the proposed techniques required a surface for which all attributes were known and could be controlled.
- the lack of a sufficient number of actual patient data sets made it difficult to produce statistically meaningful results.
- the patient data that was available was produced by a relatively new system. The transformation of this data into a suitable input form was still in the experimental stage with a number of factors that could be adjusted. It was unclear as to the appropriate settings of these factors and what the consequences of certain choices would be.

A cylinder was chosen for the test function since it provides two easily identifiable principal axes, has a simple shape classification, can be easily scaled, and has a known curvedness quantity. Data for the cylinder was generated from an equation to allow for ease in changing sampling density, orientation, and radius. The cylinder was also

used because it resembled the back surface. The major shape regions of a typical back surface are two ridges separated by a trough. This could be represented by the top halves of two cylinders separated by the bottom half of another. Other functions were used to test the ability of the techniques to determine appropriate shape regions but only the cylinder was used to test the robustness of methods.

## 6.4 Rotation invariance

If the back surface data set is considered to be a collection of points in the x-y plane, rotation tests were performed about the z-axis and the x-axis. The z-axis rotation can be related to the lateral sway of the patient while the x-axis rotation can be related to the front-to-back “rocking” motion.

### 6.4.1 Surface area

The first test of invariance to rotation examined the estimated surface area measurement. The formula used for the estimated surface area was not exactly as that provided earlier i.e.  $s_{area} \approx \sqrt{E G - F^2}$ . A shape that is to be rotated and represented on a discrete grid will always suffer aliasing inaccuracies. A simple line drawn to the same length but viewed at two different angles on a discrete grid will in general not be composed of the same number of discrete points. Therefore, it can not be expected that an arbitrarily shaped region will always have the same number of samples within its bounds as it undergoes rotation. To compensate for this the estimated surface area is normalized by dividing its value by the number of samples used to obtain the

deg.	area	deg.	area
0.0	1.0019	35.0	1.00163
5.0	1.00157	40.0	1.00161
10.0	1.00172	45.0	1.00152
15.0	1.00169	50.0	1.00161
20.0	1.00169	55.0	1.00162
25.0	1.00163	60.0	1.00164
30.0	1.00164	65.0	1.00163

Table 6.1: Normalized, estimated surface area of a cylinder undergoing z-axis rotation

deg.	area	deg.	area
0.0	1.0019	20.0	1.00639
5.0	1.00318	25.0	1.00794
10.0	1.00388	30.0	1.00953
15.0	1.00499		

Table 6.2: Normalized, estimated surface area of a cylinder undergoing x-axis rotation

quantity -  $s_{area} \approx \sqrt{EG - F^2}/N$ .  $N$  typically varies from 1 to 300 but depends on the segmentation method used and the density of the surface being examined. This normalization makes the surface area estimation independent of scaling as well. The results of the rotation tests are shown in tables 6.1 and 6.2. The normalized surface area has an average value of 1.00165 with a maximum deviation of  $\pm 0.0025$  or 0.25% for the z-axis rotation tests. For the x-axis rotation tests the difference was almost as insignificant with a maximal difference of 0.76%. Comparison of actual surface area and the normalized surface area estimate is not suggested since the comparison would not be limited to determining the accuracy of the implementation, but of the estimation method as well. Consequently, surface area should be regarded as having the units of  $units^2$ .



### 6.4.2 Principal curvature directions

The principal curvatures,  $\kappa_1$  and  $\kappa_2$  are vectors and as such have a magnitude and a direction. To simplify comparison, the magnitudes have been normalized with the magnitude of  $\kappa_1$  set to one resulting in  $\kappa_2$  being equal to the ratio  $\kappa_2/\kappa_1$ . During the tests from which the surface area rotation data was collected, the angles of the principal curvatures were also measured. Recall that curvature can be visualized as the inverse of the radius of a circle that best approximates the tangent at a point. The maximum curvature of a cylinder is then related to its radius, with the minimum curvature having a value of zero. The minimum curvature is zero since it requires a circle of infinite radius to approximate the flat tangent along the length of the cylinder. The angles of the principal curvatures for a cylinder are 90 degrees apart. Figures 6.8 and 6.9 compare the measured principal curvature angles with the known angles of the rotated cylinder. The maximum curvature angle in this was equal to the angle of rotation ( $y = x$ ). Using a least squares fitting method, the experimental data best fit the equation  $y = 1.0397x - 1.1812$  with a correlation of 0.99936. For the minimum curvature angle the theoretical relationship was  $y = x - 90$ . The experimental data fit the equation  $y = 1.0237x - 91.2477$  with a correlation of 0.99915.

All of the above rotation tests involved rotations within the plane of the image. That is, if the data set is considered to be a collection of points on the x-y plane, rotations were solely around the z-axis. Another test, conducted to examine the effect of rotating the data about the x-axis angles, found that there was no measureable difference in the calculated principal curvature angles.

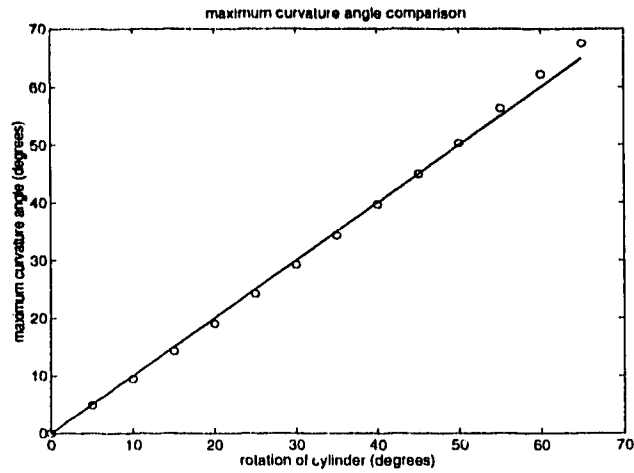


Figure 6.8: Maximum curvature angle compared to cylinder rotation angle

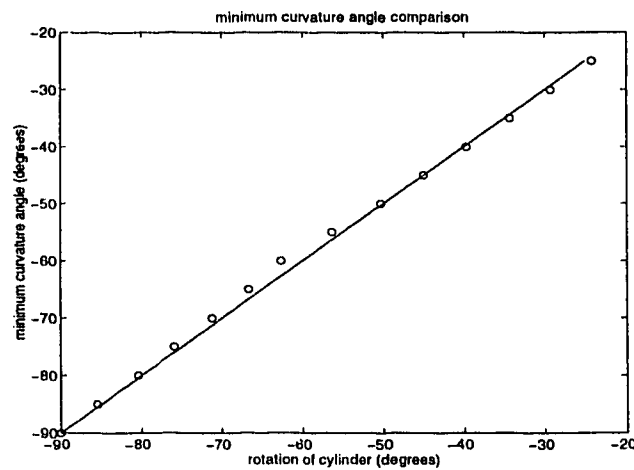


Figure 6.9: Minimum curvature angle compared to cylinder rotation angle

### 6.4.3 Curvedness

In addition to rotation invariance, the measured quantities were intended to be invariant to scale. To capture the size attribute of a region, curvedness was suggested by Koenderink and van Doorn[26]. Curvedness should also be invariant to rotation since any region, regardless of size could have a change in orientation. Table 6.3 shows that for the cylinder test data the curvedness is essentially constant and therefore invariant

to rotation about the z-axis. The value of curvedness for a cylinder with radius equal to one, is  $c = 1/\sqrt{2}$ . There was a slight change in the value of curvedness for rotation

deg.	curvedness	deg.	curvedness
0.0	0.707107	35.0	0.707107
5.0	0.707107	40.0	0.707107
10.0	0.707107	45.0	0.707107
15.0	0.707107	50.0	0.707107
20.0	0.707108	55.0	0.707107
25.0	0.707108	60.0	0.707107
30.0	0.707107	65.0	0.707108

Table 6.3: Curvedness measure of cylinder undergoing z-axis rotation

about the x-axis. Figure 6.10 shows an increasing trend in the value of curvedness but even at 30°, the percentage difference is less than 0.005%. Koenderink and van Doorn

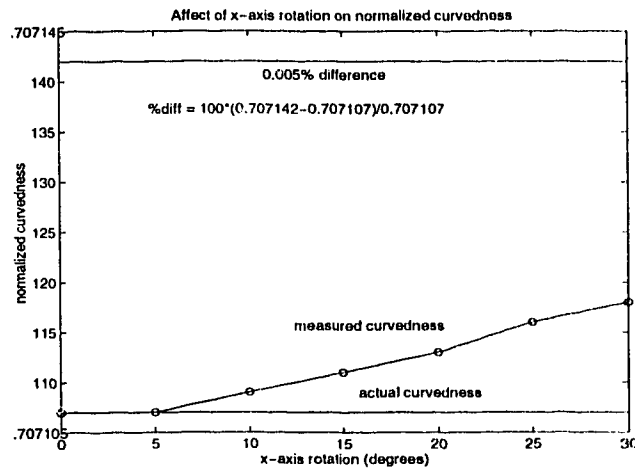


Figure 6.10: Curvedness measure of cylinder undergoing x-axis rotation

[26] related curvedness to scale. The first implementation of their curvedness definition did indeed provide a measure of scale but it was also found to be dependent on the width of the Gaussian used ( $\sigma$ ). To remove the dependence on  $\sigma$ , the formula for calculating curvedness was adjusted which resulted in the normalized version shown

below:

$$c = \sqrt{\frac{1 + \left[ \frac{\sum \kappa_1}{\sum \kappa_2} \right]^2}{2}} \quad (6.1)$$

The summations involve all of the sample values within the region of interest.

## 6.5 Scale invariance

To test for scale invariance, the radius of the test cylinder was incremented from 5 units to 50 units.

### 6.5.1 Surface area

The normalized surface area measure increased slightly with increasing cylinder radius. While experiencing a change of scale of a factor of 10, the normalized surface area only experienced a 0.15% change. A graph of the results is shown in figure 6.11.

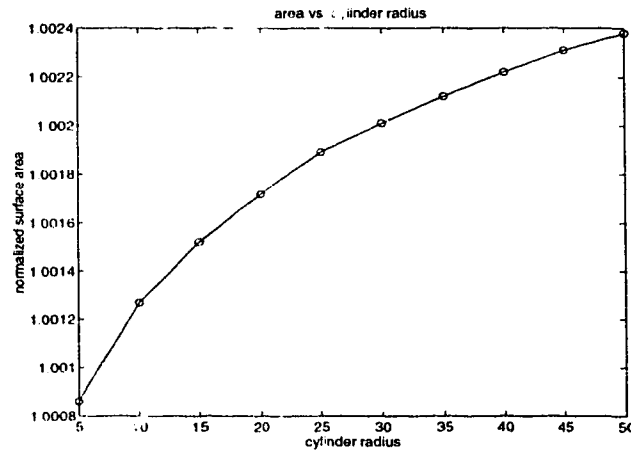


Figure 6.11: Normalized surface area as affected by scale changes

### 6.5.2 Principal curvature directions

The principal axes were also examined for invariance to scale changes. As shown in figure 6.12, the maximum curvature angle improved in accuracy as the radius of the cylinder was increased. Figure 6.13 shows that the minimum curvature angle remained relatively consistent within a  $\pm 2.0\%$  tolerance with the exception of a few points. Including these points the change in the minimum curvature angle was within  $\pm 4\%$  of the actual value of  $-80^\circ$ . Besl [8] did not propose to use these angles as surface characteristics because he considered them to be very sensitive to noise. The behavior of the minimum principal curvature angle could be related to this problem with noise.

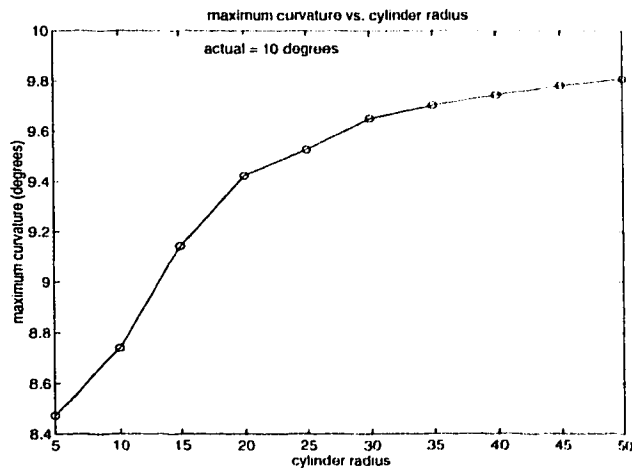


Figure 6.12: Maximum curvature angle as affected by scale changes

### 6.5.3 Curvedness

The normalized curvedness measure remained very stable as the radius of the cylinder was increased. In fact, there was no measurable difference over the entire scale of

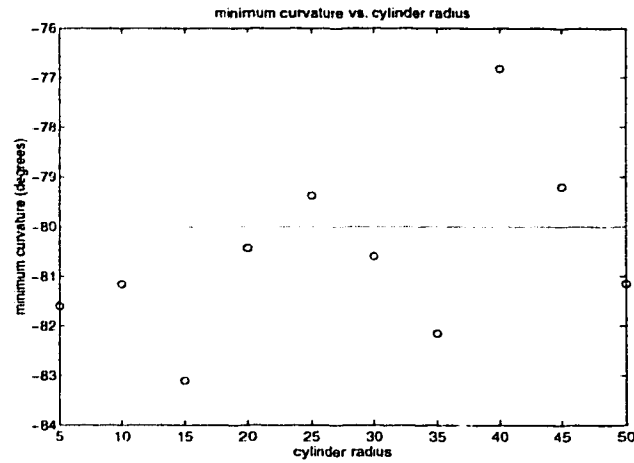


Figure 6.13: Minimum curvature angle as affected by scale changes

radius as can be seen by examining the results shown in table 6.4.

radius	curvedness	radius	curvedness
5.0	0.707107	30.0	0.707107
10.0	0.707107	35.0	0.707107
15.0	0.707107	40.0	0.707107
20.0	0.707107	45.0	0.707107
25.0	0.707107	50.0	0.707107

Table 6.4: Curvedness measure of cylinder undergoing scale change

## 6.6 Gaussian width effects

The width of the Gaussian plays an important part in the effectiveness of the kernel for use in determining partial derivatives. Ideally all of the measurements made for use in comparisons would not be affected by the value chosen for  $\sigma$ . However,  $\sigma$  and kernel size are primary implementation considerations. The choice of  $\sigma$  was examined to see how various measurements were affected.

### 6.6.1 Surface area

Table 6.2 showed how normalized surface area was practically invariant to x-axis rotation. The cylinder data was also used to examine surface area for a range of  $\sigma$  values. A separate test was conducted on a slightly rotated cylinder ( $10^\circ$ ) for the same  $\sigma$  range to see if surface area was still invariant to rotation. Figure 6.14 shows that invariance to rotation is dependent on  $\sigma$  selection. Figure 6.15 shows the

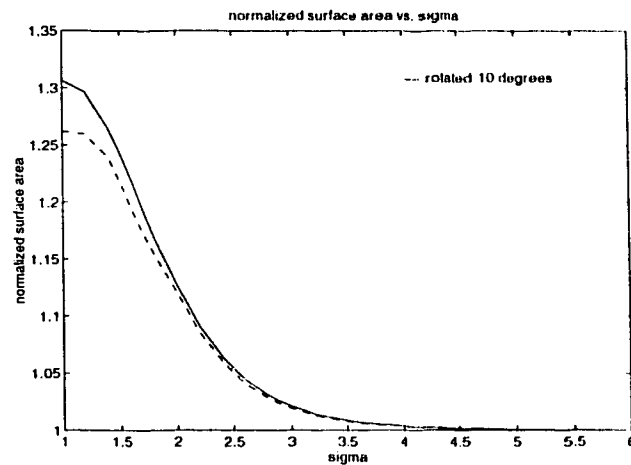


Figure 6.14: Gaussian width effects on estimated surface area

difference between the surface areas for the rotated and non-rotated cylinder as  $\sigma$  is increased. The largest discrepancy is only 3.45% but this is still much larger than the 0.25% difference in surface area due to rotation alone. For an error less than 1%, the choice of  $\sigma$  should be greater than 2.0.

### 6.6.2 Principal curvatures

The relationships between the principal curvature angles and the Gaussian width are shown in figures 6.16 and 6.17. The maximum curvature angle seems to be susceptible

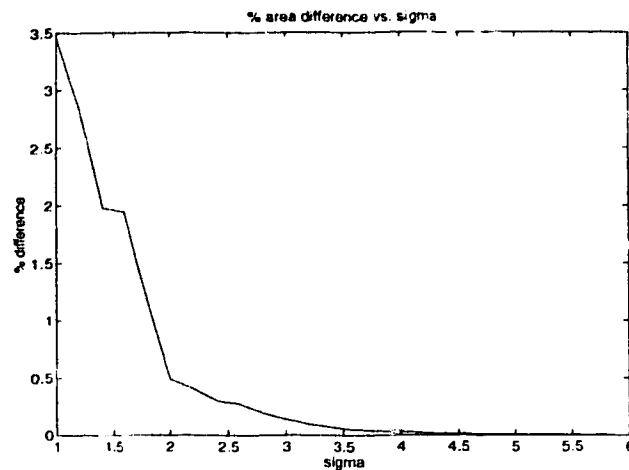


Figure 6.15: Percentage difference between rotated and non-rotated cylinder surface areas as affected by choice of  $\sigma$ .

to low values of  $\sigma$  while the minimum curvature angle seems susceptible to higher values of  $\sigma$ . A line has been drawn on figure 6.17 at  $\sigma \approx 3.8$  to show where the volume of the Gaussian kernel falls below 90% ( kernel size =  $7 \times 7$  ). The inaccuracy of the values within the kernel may be a cause for the erratic behavior of the minimum curvature angle after this point. For the maximum curvature angle, the choice of  $\sigma$  suggested from figure 6.15 (  $\sigma > 2.0$  ) would eliminate the erratic values associated with smaller  $\sigma$  values.

### 6.6.3 Curvedness

Changing the width of the Gaussian used in creation of the convolution kernel had no effect on the value of the normalized curvedness. The testing of  $\sigma$  in the range 1.0 to 5.8 did not affect the calculated curvedness for the cylinder data.



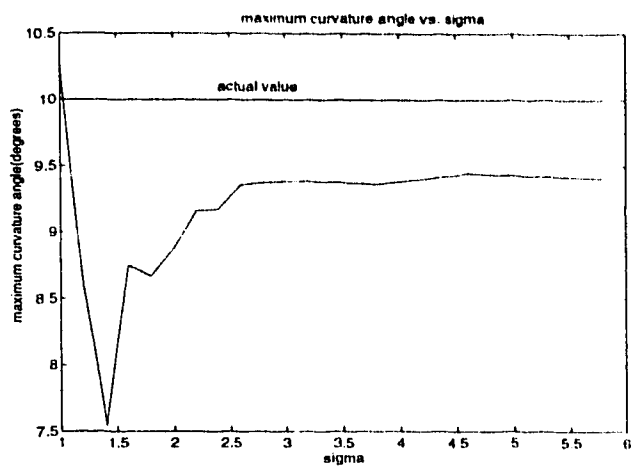


Figure 6.16: Affect of sigma on the maximum principal curvature angle

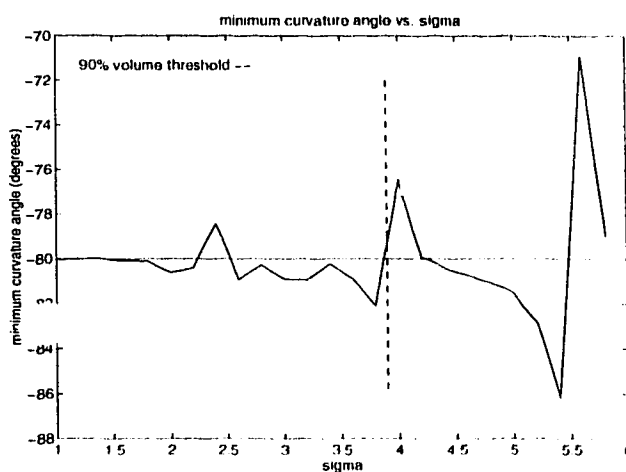


Figure 6.17: Affect of sigma on the minimum principal curvature angle

#### 6.6.4 Shape classification

The width of the Gaussian directly affects the visual appearance of the shape classification regions. Larger values of  $\sigma$  mean that more samples will have a larger effect on the end value of an operation. This is visually seen in the creation of larger, more homogeneous shape regions as shown in figure 6.18.

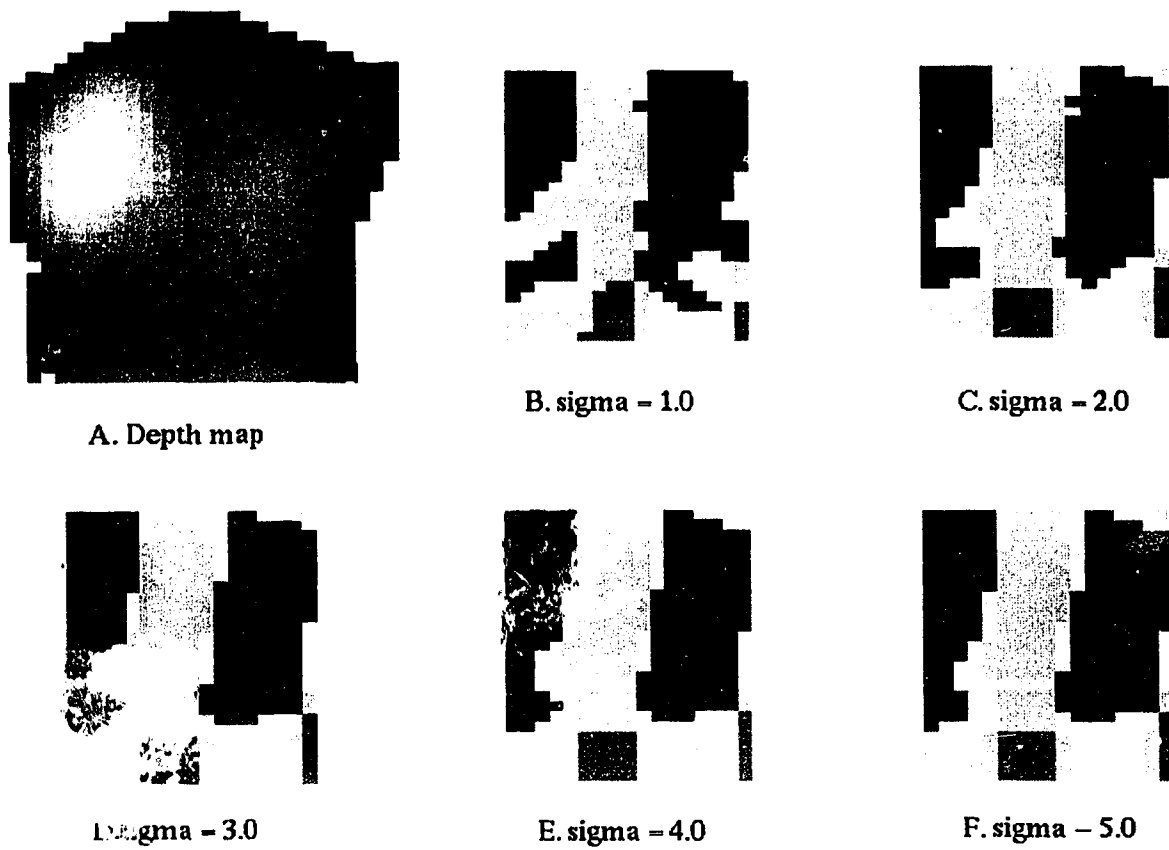


Figure 6.18: A) Depth map, B) - F) are H and K shape maps created by varying the Gaussian width

# Chapter 7

## Conclusions

The objective of this work was to find and implement techniques that would allow for the monitoring of change in the appearance due to scoliosis as seen on the surface of the back. Segmentation of the back surface into regions of similar shape was performed as a first step to reduce the number of areas which could be monitored. A number of shape classifications were suggested: Gaussian and mean curvature, sign of curvatures, and shape index. Determining the surface curvature values required a method for calculating discrete partial derivatives. Two methods were examined: the directional derivative method as used by Frobin [40] and the Gaussian convolution method as used by Witkin [44], Koenderck and van Doorn [26],[25], Babaud [21] and Blom [24]. The directional derivative approach suffered from a number of problems. One problem was its inability to produce suitably homogeneous shape regions, possibly related to its poor first partial derivative approximation as presented earlier. Another problem was the effect of rotation on the approximated partial derivatives. While attempting to gather test results it was noticed that for rotated data the re-

sulting shape regions were extremely noisy - there was a visible lack of homogeneity. As mentioned previously, homogeneous shape regions are crucial to determining any results since regions are formed as continuous groupings of similarly-valued samples. Fortunately, the Gaussian convolution approach was able to provide adequate approximations for the partial derivatives that were not affected by rotation or scaling.

Changes in regions were examined by rotating and scaling test data and recording the effects on curvedness, surface area, and the angles of the principal curvatures. Curvedness was found to be very stable and was invariant to changes in rotation and scaling. Normalized surface area and the principal curvature angles experienced little change as a result of rotation and scaling but were found to have a dependence on the width of the Gaussian used in the convolution kernel. A range of  $\sigma$  which minimized this dependency was determined to be  $\sigma \in (2.0, 4.0)$ . This range applied to the use of a kernel that was  $7 \times 7$ . A larger kernel would allow a larger  $\sigma$  as the upper bound.

The use of colour to identify shape classifications was added to help the operator interpret the segmented images. The colour labelling technique suggested by Koenderink and van Doorn [26] has been developed with ease of identification in mind and it is hoped that users of the system developed in part with this work will find the colour scheme to be intuitive.

# Chapter 8

## Future Work

This work provides a good basis for the analysis of change in the scoliotic back surface. In order to improve its usefulness as a possible diagnostic tool, work should continue in both the calculation of the quantitative results and in the clinic. For the software program the following areas should be investigated:

- removal of  $\sigma$  dependence from surface area and principal curvature angles.
- find other invariant quantities to describe the shape regions
- find an alternate kernel which does not require  $3 \times 3$  convolutions to produce an approximation to the second partial derivative. This would allow use of a larger kernel if necessary with the same loss of edge data as the current implementation. One possible kernel design technique is offered by Weiss' power-preserving filters [42].

On the clinical side, many back surface data sets need to be examined to test the practical values of curvedness, normalized surface area, and the principal curvature

angles as measures of change. Also, the type of shape representation which provides the best results needs to be determined. From the tests conducted in this work it would seem that the shape index classification offers the most discrimination between shape types but it may be too much discrimination for practical use. Lastly, if an alternate kernel technique is not found, further usage of the program with clinical data may help to find a suitable  $\sigma$  value which provides good results for most back surface analyses.

## Bibliography

- [1] M. Abramowitz and I. Stegun. *Handbook of Mathematical Functions with Formulas, Graphs, and Mathematical Tables*. Dover Publications, New York, 1968.
- [2] F. Arman and J. K. Aggarwal. Dense-range images. *ACM Computing Surveys*, 25(1):12–37, March 1993.
- [3] F. Attneave. Some informational aspects of visual perception. *Psychol. Rev.*, 61(3), 1954.
- [4] W. Frobin B. Drerup and E. Hierholzer. Computerized evaluation of surface measurements of kyphosis and scoliosis. *Moire Fringe Topography*, pages 155–163, 1983.
- [5] J. J. Koenderink B. M. ter Haar Romeny, L. M. J. Florack and M. A. Viergever. Invariant third order properties of isophotes: T-junction detection. In *Proceedings, Scand. Conf. on Image Analysis*, pages 30–37, Aalborg, DK, August 13–16 1991.
- [6] John R. Bennett and John S. MacDonald. On the measurement of curvature in a quantized environment. *IEEE Transactions on Computers*, 24(8):803–819,

August 1975.

- [7] Paul Besl and Ramesh Jain. Three-dimensional object recognition. *ACM Computing Surveys*, 17(1):75-145, March 1985.
- [8] Paul Besl and Ramesh Jain. Intrinsic and extrinsic surface characteristics. *IEEE Trans. Pattern Anal. Mach. Intell.*, 8(1):26-33, January 1986.
- [9] Paul Besl and Ramesh Jain. Invariant surface characteristics for 3d object recognition in range images. *Computer Vision, Graphics & Image Processing*, 33(1):33-80, 1986.
- [10] Paul Besl and Ramesh Jain. Segmentation through variable-order surface fitting. *IEEE Transactions on Pattern Anal. Mach. Intell.*, 10(2):167-192, March 1988.
- [11] J. R. Cobb. Outline for the study of scoliosis. *The Academy of Orthopaedic Surgeons, Instructional Course Lectures*, 5, pages 261-275, 1948.
- [12] Thomas S. Huang Dmitry B. Goldgof and Hua Lee. Feature extraction and terrain matching. In *Proceedings, CVPR '88*, pages 899-904, June10-13 1988.
- [13] B. Drerup and E. Hierholzer. Detection of anatomical landmarks on the back surface: The vertebra prominens as a region of extreme curvature. *Surface Topography and Spinal Deformity*, pages 151-157, 1986.
- [14] Patrick J. Flynn and Anil K. Jain. On reliable curvature estimation. In *Proceedings, CVPR '89*, pages 110-116, San Diego, CA, June4-8 1989.



- [15] W. Frobin and E. Hierholzer. Analysis of human back shape using surface curvature. *Journal of Biomechanics*, 15(5):379–390, 1982.
- [16] Gaille G. Gordon. Face recognition based on depth and curvature features. In *Proceedings, IEEE Computer Vision and Pattern Recognition*, pages 808–810, June 1992.
- [17] E. Hierholzer and B. Drerup. Shape analysis of the back surface: Automatic localization of anatomical landmarks and assessment of lateral asymmetry. *Surface Topography and Spinal Deformity IV*, pages 267–274, 1987.
- [18] D. Hilbert and S. Cohn-Vossen. *Geometry and the Imagination*. Chelsea, New York, 1952.
- [19] M. H. Pope I. A. F. Stokes, M. S. Moreland and J. G. Armstrong. Correlation of back survey topography with 3-d spine shape in scoliosis. *Moire Fringe Topography*, pages 61–67, 1983.
- [20] David J. Ittner and Anil K. Jain. 3-d surface discrimination from local curvature measures. In *Proceedings, CVPR '85*, pages 119–123, San Francisco, CA, June 10–13 1985.
- [21] M. Baudin J. Babaud, A. P. Witkin and R. O. Duda. Uniqueness of the gaussian kernel for scale-space filtering. *IEEE Trans. Pattern Anal. Mach. Intell.*, 8(1):26–33, January 1986.

- [22] A. R. Turner-Smith J. D. Harris, R. J. Jefferson and D. Thomas. Transverse asymmetry, a measure of the progression of scoliosis. *Surface Topography and Spinal Deformity IV*, pages 85–94, 1987.
- [23] M. Moreau J. Raso, B. Greenhill and D. Budney. The combined reconstruction of spinal and surface deformity. *Surface Topography and Spinal Deformity*, pages 13–20, 1987.
- [24] Bart M. ter Haar Romeny Johan Blom and Jan J. Koenderink. Spatial derivatives and the propagation of noise in gaussian scale space. *Journal of Visual Communications and Image Representation*, 4(1):1–13, March 1993.
- [25] J. J. Koenderink. The structure of images. *Biol. Cybernetics*, 1(50):363–370, January 1984.
- [26] J. J. Koenderink and A. J. van Doorn. Surface shape and curvature scales. *Image and Vision Computing*, 10(8):557–565, November 1992.
- [27] J. J. Koenderink L. M. J. Florack, B. M. ter Haar Romeny and M. A. Viergever. Cartesian differential invariants in scale-space. *Journal of Mathematical Imaging and Vision*, 3:327–348, 1993.
- [28] Richard Liu. Three dimensional reconstruction of trunk surface using structured light. Master's thesis, University of Alberta, Electrical Engineering Department, 1995.

- [29] Jan J. Koenderink, Luc M. J. Florack, Bart M. ter Haar Romeny and Max A. Viergever. Scale and the differential structure of images. *IEEE CVPR*, 10(8):557–565, November 1992.
- [30] Don Mitchell and Pat Hanrahan. Illumination from curved reflectors. *Computer Graphics*, 26(2):283–291, 1992.
- [31] Roland Penner. Realistic computer visualization of three dimensional data. Master's thesis, University of Alberta, Electrical Engineering Department, 1995.
- [32] G. C. Santambrogio, R. Assente, A. Pedotti and A. Cometti. An automatic non-invasive system for the analysis of spinal deformity. *Surface Topography and Spinal Deformity*, pages 61–69, 1986.
- [33] G. Schumpe and H. Messier. Comparison of parameters used for the measurement of spinal deformity by means of optometric, ultrasonic and radiographic technique. *Surface Topography and Spinal Deformity IV*, pages 203–221, 1987.
- [34] C. E. Shannon. Prediction and entropy of printed english. *Bell Syst. Tech. J.*, 30:50–64, 1951.
- [35] James Stewart. *Calculus*. Brooks/Cole, Monterey, California, 1987.
- [36] Alexander M. Taratorin and Samuel Sideman. Constrained regularized differentiation. *IEEE Trans. Pattern Anal. Mach. Intell.*, 16(1):88–92, January 1994.

- [37] Emmanuele Trucco and Robert B. Fisher. Experiments in curvature-based segmentation of range data. *IEEE Trans. Pattern Anal. Mach. Intell.*, 17(2):177–182, February 1995.
- [38] A. R. Turner-Smith and J. D. Harris. Isis - an automated shape measurement and analysis system. *Surface Topography and Spinal Deformity*, pages 31–38, 1986.
- [39] Alan R. Turner-Smith and David C. Thomas. Some relationships between the spine and skin surface. *Surface Topography and Spinal Deformity IV*, pages 3–11, 1987.
- [40] E. Hierholzer W. Frobin and B. Drerup. Shape analysis of surfaces: Extraction of shape from coordinate data. *Moire Fringe Topography and Spinal Deformity*, pages 71–82, 1983.
- [41] J. Wegner. Measurement of scoliosis deformity using moire topography. Master's thesis, University of Alberta, Mechanical Engineering Department, 1985.
- [42] Isaac Weiss. Higher-order differentiation filters that work. *IEEE Transactions on Pattern Analysis and Machine Intelligence*, 16(7):734–739, July 1994.
- [43] G. Windischbauer and H. Neugebauer. The analysis of human back shape asymmetries by computer algorithms. *Surface Topography and Spinal Deformity IV*, pages 259–265, 1987.

- [44] A. P. Witkin. Scale space filtering. In *Proc. IJCAI*, pages 1019–1023, Karlsruhe, West Germany, January 1983. Academic Press.

# Appendix 1

## Vector Mathematics

### 1.1 Vector Definition

**vector:** a quantity that has both a magnitude and a direction. A vector in n-dimensional space can be represented as an ordered n-tuple where each component of the n-tuple is the magnitude in that direction. For the three-dimensional case vectors can be expressed as:  $\vec{v} = \langle v_x, v_y, v_z \rangle$ , where the standard Cartesian coordinate reference frame is being used.

### 1.2 Vector Operations

Addition

$$\vec{a} + \vec{b} = \vec{c} = \langle a_x + b_x, a_y + b_y, a_z + b_z \rangle$$

Subtraction

$$\vec{a} - \vec{b} = \vec{c} = \langle a_x - b_x, a_y - b_y, a_z - b_z \rangle$$

Magnitude

$$|\vec{\mathbf{a}}| = \sqrt{a_x^2 + a_y^2 + a_z^2}$$

Dot product

$$\vec{\mathbf{a}} \cdot \vec{\mathbf{b}} = \vec{\mathbf{c}} = a_x * b_x + a_y * b_y + a_z * b_z$$

# Appendix 2

## Discrete Convolution

The continuous convolution operation for two functions  $f(x,y) * g(x,y)$  is defined as,

$$f(x,y) * g(x,y) = \int_{-\infty}^{\infty} \int_{-\infty}^{\infty} f(\alpha,\beta)g(x - \alpha, y - \beta) d\alpha d\beta.$$

The two-dimensional discrete convolution relationship is similarly defined. Let  $f(x,y)$  and  $g(x,y)$  be two discrete arrays of size  $A \times B$  and  $C \times D$  respectively. For discrete functions periods are assumed in both the  $x$  and  $y$  directions. The periodic nature of discrete functions is evident when they are examined in the Fourier domain.

To avoid the wrapping effect of circular convolution, the periods in the  $x$  and  $y$  directions for the resultant function are chosen as

$$M \geq A + C - 1$$

and

$$N \geq B + D - 1$$



$$f(x, y) * g(x, y) = \sum_{m=0}^{M-1} \sum_{n=0}^{N-1} f(m, n)g(x - m, y - n)$$

# Appendix 3

## Discrete derivative kernels

Let  $S$  be a surface expressed as a collection of discrete points  $S(i,j)$ . Using a 3x3 neighbourhood centered about a point, an approximation to the curvature at that point can be determined. The surface vectors for the neighbourhood  $g_{i,j}$  are created as follows: (  $h$  is the sampling distance )

$$g_{i,j} = \langle i, j, S(i, j) \rangle$$

$$g_{i+1,j} = \langle i + h, j, S(i + h, j) \rangle$$

$$g_{i-1,j} = \langle i - h, j, S(i - h, j) \rangle$$

$$g_{i,j-1} = \langle i, j - h, S(i, j - h) \rangle$$

$$g_{i,j+1} = \langle i, j + h, S(i, j + h) \rangle$$

$$g_{i+1,j+1} = \langle i + h, j + h, S(i + h, j + h) \rangle$$

$$g_{i+1,j-1} = \langle i + h, j - h, S(i + h, j - h) \rangle$$

$$g_{i-1,j+1} = \langle i-h, j+h, S(i-h, j+h) \rangle$$

$$g_{i-1,j-1} = \langle i-h, j-h, S(i-h, j-h) \rangle$$

Using these vectors, the approximations to the derivatives of the surface are:

$$x_u = \frac{1}{6h}(g_{11} - g_{-11} + g_{10} - g_{-10} + g_{1-1} - g_{-1-1})$$

$$x_v = \frac{1}{6h}(g_{-11} - g_{-1-1} + g_{01} - g_{0-1} + g_{11} - g_{1-1})$$

$$x_{uu} = \frac{1}{3h^2}(g_{10} + g_{-10} + g_{11} + g_{-11} + g_{1-1} + g_{-1-1} - 2(g_{00} + g_{01} + g_{0-1}))$$

$$x_{uv} = \frac{1}{4h^2}(g_{11} - g_{-11} + g_{-1-1} - g_{1-1})$$

$$x_{vv} = \frac{1}{3h^2}(g_{01} + g_{0-1} + g_{11} + g_{1-1} + g_{-11} + g_{-1-1} - 2(g_{00} + g_{10} + g_{-10}))$$

Substituting in the vectors  $g_{i,j}$  yields:

$$x_u = \langle 1, 0, \frac{1}{6h}(S(i+h, j+h) - S(i-h, j+h) + S(i+h, j) - S(i-h, j) + S(i+h, j-h) - S(i-h, j-h)) \rangle$$

$$x_v = \langle 0, 1, \frac{1}{6h}(S(i-h, j+h) - S(i-h, j-h) + S(i, j+h) - S(i, j-h) + S(i+h, j+h) - S(i+h, j-h)) \rangle$$

$$x_{uu} = \langle 0, 0, \frac{1}{3h^2}(S(i+h, j) + S(i-h, j) + S(i+h, j+h) + S(i-h, j+h) + S(i+h, j-h) + S(i-h, j-h) - 2S(i, j) - 2S(i, j+h) - 2S(i, j-h)) \rangle$$

$$x_{uv} = \langle 0, 0, \frac{1}{4h^2}(S(i+h, j+h) - S(i-h, j+h) + S(i-h, j-h) - S(i+h, j-h)) \rangle$$

$$\begin{aligned}
x_{vv} = & \langle 0, 0, \frac{1}{3h^2} (S(i, j+h) + S(i, j-h) + S(i+h, j+h) \\
& + S(i+h, j-h) + S(i-h, j+h) + S(i-h, j-h) \\
& - 2S(i, j) - 2S(i+h, j) - 2S(i-h, j)) \rangle >
\end{aligned}$$

Gaussian curvature K of the surface can be determined using:

$$E = x_u \cdot x_u$$

$$F = x_u \cdot x_v$$

$$G = x_v \cdot x_v$$

$$L = n \cdot x_{uu}$$

$$M = n \cdot x_{uv}$$

$$N = n \cdot x_{vv}$$

$$K = \frac{LN - M^2}{EG - F^2} \quad (3.1)$$

where n is defined as

$$n = \frac{x_u \times x_v}{|x_u \times x_v|}$$

To simplify notion, I will refer to the x,y and z components of a vector as vector.component. For instance, the z component of the vector  $x_u$  would be  $x_u.z$ .

Evaluating for E, F, and G yields:

$$E = 1 + (x_u.z)^2 \quad (3.2)$$

$$F' = (x_u, z)(x_v, z) \quad (3.3)$$

$$G = 1 + (x_v, z)^2 \quad (3.4)$$

Solving for the normal vector n ...

$$n = \frac{\langle -x_u, z, -x_v, z, 1 \rangle}{\sqrt{(x_u, z)^2 + (x_v, z)^2 + 1}}$$

Now evaluating for L, M, and N ...

$$L = \frac{x_{uu}, z}{\sqrt{(x_u, z)^2 + (x_v, z)^2 + 1}} \quad (3.5)$$

$$M = \frac{x_{uv}, z}{\sqrt{(x_u, z)^2 + (x_v, z)^2 + 1}} \quad (3.6)$$

$$N = \frac{x_{vv}, z}{\sqrt{(x_u, z)^2 + (x_v, z)^2 + 1}} \quad (3.7)$$

Substituting equations 3.3 through 3.7 into equation 3.1 to solve for K yields:

$$K = \frac{(x_{uu}, z)(x_{vv}, z) - (x_{uv}, z)^2}{((x_u, z)^2 + (x_v, z)^2 + 1)^2} \quad (3.8)$$